Impact of Planar Microcavity Effects on Light Extraction—Part I: Basic Concepts and Analytical Trends

H. Benisty, H. De Neve, and C. Weisbuch

Abstract—We address the long-standing issue of extracting light as efficiently as possible from a high-index material, $n \geq 2$, where as little as 2%–10% of light not suffering total internal reflection is extracted at standard plane faces due to the small critical angle $\sim 1/n$. Using a planar microcavity to redirect spontaneous emission toward the surface, constructive interferences can bring 15%–50% of the light out, enhancing brightness and efficiency. In this first of two papers, an approximate approach is used showing the importance of small cavity order m_c and of the m_c/n^2 ratio. We define a condition for microcavity regime as $m_c < 2n^2$. It is shown that most of light extraction is usually attained for moderate mirror reflectivities $\sim 1 - m_c/n^2$ typically below 90%, and without strong directionality. Balance between emission directionality, radiance (brightness), and spectral narrowing is discussed. We define a brightness enhancement factor B given by $Bm_c\Delta\Omega = 4\pi$ where $\Delta\Omega$ is the largest internal solid angle of either the cavity mode or that deduced from the material emission linewidth. Design rules are applied to distributed dielectric mirrors yielding an optimal number of periods. The underlying physical competition between emission into guided modes, Fabry–Perot modes and the so-called "leaky modes" is analyzed.

Index Terms— Cavities, distributed feedback devices, Fabry–Perot resonators, light-emitting diodes, light sources, microcavities, semiconductor device modeling, semiconductor films.

NOMENCLATURE

$A_{\text{guid}}, A_{\text{leak}}$	Fraction of emission into guided and leaky modes.
Airy	Airy function.
B	Brightness enhancement over the no-cavity case.
c	Light velocity.
D	Airy function denominator
$D_{\min}$	Minimum value of D.
E	Electric field.
f_g, f_{lk}, f_m	Fraction of power in guided modes, leaky modes and in metal (II).
F	Cavity finesse.
k	Wavevector of light in the medium.
k_o	Central emission wavevector in the medium.
L	Cavity thickness.
L_p	Penetration length in DBR mirrors.
m	Reduced distance in half-wavelength units.
m_o	Bare cavity order, not including penetration length into mirrors.
m_c	Cavity order, including penetration length into DBR mirrors.
n	Optical index of semiconductor or cavity.
n_{hi}	High index in DBR mirrors.
n_{lo}	Low index in DBR mirrors.
n_{mid}	Average index in DBR mirrors.
n_{out}	Outside medium index.
P_o, P_{lk}, P_g	Powers in the outside, leaky and guided modes, per dipole (II).
P_{tot}	Total power emitted including lifetime modification, normalized to no-cavity case (II).
p, p_{opt}	Number of stack pairs (periods) in DBR mirror, optimal number.
r_1	Top mirror amplitude reflectivity.
R_1	Top mirror power reflectivity.
r_2	Bottom mirror amplitude reflectivity.
R_2	Bottom mirror power reflectivity.
s	Relative detuning of emission.
S	Natural emission relative spectral width (natural linewidth).
S_{esc}	Threshold relative spectral width for linewidth-limited extraction
T_1	Top mirror transmission.
v	Ratio of cavity order to squared index.
v_{infl}	Location of inflexion points in the (η, v) plane.
z	Source location in the cavity.
2ϕ	Round-trip phase in the cavity.
$2\phi'$	Relative phase of reflected beam on bottom mirror.
Δk	Natural emission width in terms of wavevector.
Δm_c	Increase in cavity order due to distributed mirrors.
Δn	Index step of distributed mirrors
$\Delta\theta$	Inside lobe angular width.
$\Delta\theta'$	Outside lobe angular width.
$\Delta\Omega$	Inside solid angle of the lobe.
$\Delta\Omega'$	Outside solid angle of the lobe.
ζ, ζ_i	Antinode factor, same factor for the ith mode.

$\eta, \eta_{pc}, \eta_{\text{eff}}$ Extraction efficiency, extraction per cycle, effective extraction with recycling (II).

$\eta_h, \eta_v, \eta_{\text{iso}}$ Extraction efficiency of horizontal, vertical, and isotropic dipoles (II).

λ Wavelength.

$\lambda_{\text{opt}}, \lambda_B$ Wavelength of optimal extraction, Bragg wavelength of DBR mirror.

θ Angle.

θ_c Critical angle.

θ_o Smallest inside resonant angle.

θ_l Angle of stop-band edge for DBR mirrors.

θ_{lo} Critical angle for DBR low index medium.

ω Light pulsation.

Ω Solid angle.

Ω_c Internal solid angle below the critical angle.

$\Omega_{\text{gui}}, \Omega_{\text{leaky}}$ Internal solid angle of guided and leaky modes.

Meaning of some long sub and superscripts:

bare   Bare cavity, without distributed mirrors.

crit   Critical value to obtain most of the extraction enhancement.

esc   In escape window, refering to spectral width.

mono   Cavity-limited with reference to (solid) angle of lobe.

lim   Limit value between the monochromatic "mono" and "poly" cases.

loss   Optimized value of, e.g., mirror reflectivity in the presence of losses.

max   Maximum value of, e.g., extraction efficiency in the presence of losses.

poly   Spectral width-limited with reference to (solid) angle of lobe.

sp   Optimized value in the presence of spectral width.

sym   Symmetric cavity.

asym   Asymmetric cavity, with two different mirrors.

I. INTRODUCTION

S PONTANEOUS emission from solid-state sources such as semiconductors (SC's), for example, in light-emitting diodes (LED's), can often be considered internally isotropic. Since only those directions within the critical angle $\theta_c = \sin^{-1}(n_{\text{out}}/n)$ allow escape to the outer medium (n, index of semiconductor, index n_{out}, usually index of air or epoxy in commercial LED's [1], [2]), the internal solid angle $\Omega_c = 2\pi(1 - \cos\theta_c)$ for escape to air is of the order of $2\pi/2n^2$ at a planar face. For a bare source and the high indices $n = 2.5$–4 of SC media, a very small fraction $\eta_{\text{bare}} \sim 1/4n^2$ of emission may directly escape, of the order of only 2% for GaAs bandgap radiation ($n = 3.65$) [3].

Extracting the majority remainder light translates into severe technological complexity and/or material requirements: transparent substrate, surrounding of die with reflectors to redirect side-emitted light, at the expense of absolute brightness [2], [4]–[7], or extremely high internal quantum efficiency to attempt escape again through reabsorption and reemission, the mechanism known as photon recycling [8]–[12]. Another way is to redirect photon momentum through rough interfaces [13]. Instead, we discuss here what can be expected from microcavities [11], [12], [14]–[21] to alleviate the poor extraction efficiency of high-index materials retaining a simple planar structure but redirecting as many photons as possible into the escape cone by means of interferences. In the GaAs testbed case, optimized microcavity LED's at 980 nm already demonstrated $\eta = 22.8\%$ [22]–[25], prompting us to generalize this result and to determine what are the ultimate perfomances one can expect.

Microcavity effects have widely been demonstrated regarding directionality and spectral narrowing of emission from otherwise isotropic and/or broad-spectrum structures [15], [16], [21], [26]–[35]. As for total emission and hence spontaneous lifetimes, they are weakly affected for electron–hole pair recombination and the rather low reflection coefficients considered here [17], [36]–[39]. This is the so-called "weak coupling" regime, to be distinguished from the situation of exciton fluorescence in high-reflectivity cavities leading to a "strong-coupling" regime and vacuum Rabi oscillation [40]–[45]. This is also to be distinguished from the case of spontaneous emission rate enhancement by the Purcell factor $(Q/4\pi^2)(\lambda^3/V)$, occuring in three-dimensional (3-D) optical cavities of volume V and narrow emission linewidth $\Delta\lambda$ around λ, where Q is here the smallest of the quality factor or $(\lambda/\Delta\lambda)$. Focusing on the weak coupling regime, obtainment of a sharp directionality, and spectral narrowing with resonant cavities does not necessarily translate into increased extraction efficiency for the overall light emission. To increase this latter, one should gain emission in one mode at the expense of all other modes. In this respect, devices with large monochromatic brightnesses in a narrow cone rely rather on spatial and spectral features of a given mode than on the relative weight of this mode to all others.

In Section II we will in deal with a simple model of planar microcavities aimed at understanding the physics of photon redirection for an emitter inside a cavity. It is divided in many subsections dealing first with interferences seen by a source in front of a single mirror (Section II-A), switching then to cavity effect, summarizing microcavity basic formulae and stressing the need for low (micro-)cavity order to enhance extraction (Section II-B). Next, a useful "working point" suitable for lossless cavities is analyzed (Section II-C). Optimization considerations for lossy cavities follow (Section II-D), detailed in Appendix A. Spectral linewidth, directionality, and brightness, and their interplay are considered in Section II-E and Appendix B. Systems based on distributed Bragg reflector (DBR) mirrors and their leaky modes are dealt with in Section II-F and Appendix C. A brief account is made for smaller aperture requirements, e.g., for fiber coupling in Section II-G. Finally, Part II [46] complements this paper by focusing on selected exact simulations and the role of photon recycling.

II. APPROXIMATE APPROACH FOR EXTRACTION FROM A MICROCAVITY

How to extract as much light as possible from high-index spontaneously emitting materials retaining a planar structure is the issue addressed in this section from the mode structure

point of view, using a scalar approximate approach to retain simple analytical results. We will point out how the mode structure of planar stacks can be engineered to overcome the intrinsic limitation set by the higher photonic density-of-states of these materials, scaling like n^3, meaning that much more modes are found for radiation inside the material than outside. We first briefly recall here how a lossless mirror affects radiation pattern from a dipole, and in the next subsection how a cavity does. This will allow us to define what we term "close" and "far" mirror configurations and naturally focus on the first one since it is based on effects similar to those of the microcavity regime.

A. Interferences from a Single Mirror for Extraction

Let us consider a monochromatic source such as an oscillating dipole, at vacuum wavelength λ, pulsation ω, in a medium of index n, of associated wavevector $k = n\omega/c$, but located at a distance $z = m\lambda/2n$ from a planar mirror of amplitude reflectivity $\pm r_2 = \pm|R_2|^{1/2}$ close to unity with usual notations (see Fig. 1; $-r_2$ applies to metal mirrors, the case sketched in Fig. 1 for simplicity). Retaining a simpler scalar approach and neglecting lifetime, polarization, and orientational effects, the upward-radiated electric far field in the angle θ from such a dipole in front of the mirror is [47]–[49]

$$\begin{aligned} E^2 &= E_o^2|1 \pm r_2 e^{2i\phi'}|^2 \\ &= E_o^2(1 + r_2^2 \pm 2r_2\cos 2\phi') \\ &= E_o^2 \times 2\zeta \end{aligned} \tag{1}$$

where $2\phi' = 2kz\cos\theta$ for a metal-type mirror and E_o is the dipole far field without mirror. ζ is also called the antinode factor. Assuming constructive interference at normal incidence, hence $2kz = 2m\pi$ with m (half-)integer for $+(-)r_2$, $z = m\lambda/2n$, we get the two-wave interference result constructive for ϕ' even $(+r_2)$ or odd $(-r_2)$ multiple of $\pi/2$

$$E^2 = E_o^2(1 + r_2^2 \pm 2r_2\cos(2m\pi\cos\theta)). \tag{2}$$

Consider now that we collect emission within the $\theta < \theta_c$ cone with $n_{\text{out}} = 1$ for simplicity. If $m = 1/2$ (for $-r_2$, metal mirror), the dipole lies at a quarter-wave from the mirror, the r.h. factor reads $2 - 2\cos(\pi\cos\theta)$ and it remains close to $(1 + r_2)^2 \approx 4$ on the $0 \to \theta_c$ useful range since $\cos\theta > \cos\theta_c \approx 1 - 1/2n^2$ (the outside index n_{out} is taken as 1 here). It vanishes only for $\theta \approx \pi/2$, destroying light emission along the mirror plane.

Conversely, if $m > n^2$, the source is located so far that even within the small escape angles $\theta < \theta_c$, both constructive and destructive interferences occur, ϕ' deviating from $2m\pi$ by more than $-\pi/2$. Asymptotically, the mere geometric mirror effect is retained on the average

$$\langle E^2 \rangle_\theta = E_o^2(1 + r_2^2) \tag{3}$$

yielding at most a trivial factor of two on emitted power and extraction. Clearly, $m \sim n^2$ (thus $z \sim n\lambda/2$) sets the limit between what we will term "far" and "close" mirror configurations. Figures for extraction from bare, far-mirror, and close-mirror configurations and typical semiconductors are
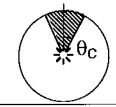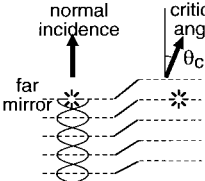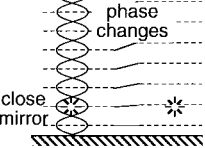

Fig. 1. Extraction efficiencies for emitter (stars) in a bare situation (top) or modified by a mirror. For an emitter lying close to a mirror (bottom), there is a negligible phase change for rays emitted between normal incidence and critical angle, unlike for an emitter far from the mirror, with a phase change larger than π (middle). Corresponding extraction efficiencies for two representative indices are indicated.

collected in Fig. 1: from $\eta_{\text{bare}} = 2\%$ in a single escape cone in GaAs-like materials ($n = 3.55$), only $\eta \sim 4\%$ are extracted in the far-mirror configuration (two cones) reaching $\eta \sim 8\%$ for the close-mirror one (when $z < 1.6\,\mu\text{m}$ for $\lambda = 900$ nm). These extractions are doubled in a higher bandgap SC of index $n = 2.55$, typically corresponding to visible green light: 4%, 8%, and 16%, respectively, (now for $z < 0.75\,\mu\text{m}$).

Let us insist that, at those particular wavelengths and angles achieving constructive interference, the mirror yields a factor of 4 on the emitted intensity for any distance $z = m\lambda/2$, even much further than $m = n^2$. The trend of monochromatic brightness is seen in this simple case to differ widely from that for global extraction, which justifies the distinction made in the introduction. Thus, the doubled extraction when $m < n^2$ arises from the larger modifications of free-space mode density in k-space (directions) enforced in the mirror vicinity. More control of the optical environment in a planar Fabry–Perot cavity is shown below to result in still improved extraction because it rests on the spectrally sharper multiple-beam spatial interference phenomenon rather than on the spectrally broader two-beam phenomenon.

B. Cavity Single-Mode Extraction: Role of the Order and Index of the Microcavity

How is emission controlled when placing dipoles in a Fabry–Perot (FP) cavity of index n and of thickness L along axis z (Fig. 2) adding a front mirror of reflectivity $R_1 = r_1^2$? Either using multiple-beam summation from an internal source, or using reciprocity of emission and absorption [39], one finds some ansatz of the Airy formula [32], [24], as explained, e.g., by Kastler [47]. It is seen in Fig. 2 that in a given direction, two series of multiple beams are to be summed, each yielding the same Airy factor. These two series
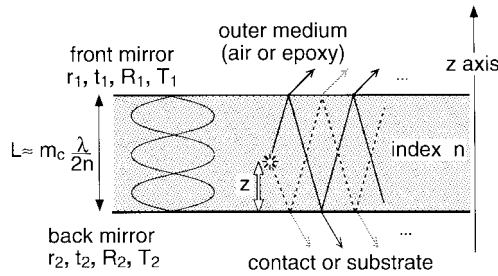
Fig. 2. Schematic cavity of index n, order m_c, limited by two mirrors, with an emitter inside emitting two series of waves.

add just as in the single-mirror case, with the same antinode factor ζ. The result reads for the upward-radiated field outside the cavity, still in a scalar view

$$|E_{\text{out}}^{\text{up}}|^2 = |E_{\text{in}}|^2 \frac{T_1 |1 + r_2 e^{2i\phi'}|^2}{|1 - r_1 r_2 e^{2i\phi}|^2}$$

$$= |E_{\text{in}}|^2 \times \zeta \times \frac{2T_1}{|1 - r_1 r_2 e^{2i\pi}|^2} \quad (4)$$

where

$$2\phi = 2kL\cos\theta \quad (5)$$

is the cavity round-trip phase and for a lossless mirror $T_1 = 1 - R_1 = 1 - r_1^2$. The separated rightmost Airy factor accounts for the cavity mode structure.

In the rigorous approach indicated in [46], a method based on internal source terms is used to calculate exactly the emission pattern of a collection of dipoles. When solving for the outside field, internal source terms also appear in a numerator, together with the above antinode factor, while the denominator is characteristic of the structure itself and is basically the same one as Airy's formula.

An obvious consequence of the peaked Airy function at large finesses is that, still more than a mirror, a cavity favors different wavelengths at different angles following the dispersion relation of quasi-modes $2\phi(\lambda, \theta) \equiv 2\pi$ (or $k \propto 1/\cos\theta$). Also, in (4), while the Airy factor yields the intrinsic enhancement/inhibition of each mode (i.e., each wavelength–angle pair), the remaining antinode factor reflects, for all modes, the coupling strength. Going from continuous to discrete modes, light emitted in guided modes can also be treated with the antinode factor for coupling strength and discrete dispersion relations $2\phi(\lambda, \theta) \equiv 2\pi$ at angles larger than θ_c.

For extraction on the top side, $R_2 = 1$ is obviously advisable to reflect the downward energy flux, and the same trends as those outlined for a single mirror apply to the antinode factor ζ: the source should lie at an antinode close from this mirror, closer than $m = n^2$. In the following, we assume for simplicity that $\zeta = 1$, the average for distributed emitters. A specific mention will be made whenever we consider, for example, a more localized source at an antinode ($\zeta = 2$).

We will define below the microcavity regime as the one where extraction is achieved through a single resonance. In order to obtain a simple description of the phenomena, we first give some practical FP formulas. We then define and

discuss the cavity order and present a k_x–k_z diagram useful to understand extraction physics in this section's approach. The next subsections specify the mirror reflectivity needed to put the microcavity to good use in extraction terms for lossless and lossy cases. This will be further applied to distributed mirror design through the increase they cause to effective cavity order.

Practical formulas $(T_1, \cdots)$ of Table I are obtained either directly from (4) or from a standard approximate development of Airy function denominator yielding a well-known Lorentzian function (see examples below). Cavity finesse F is introduced in equations (T9) [47], [50], [51] of Table I. Unless indicated, angular quantities are referred to the cavity medium. Note the singular situation of resonance exactly at normal incidence: the mode solid angle, a cone of semi-angle θ_{fwhm} in an intuitive representation, is halved compared to resonances at oblique incidence. For this latter and more general case, the mode solid angle is indeed comprised of two cones separated by $\Delta\theta$ and the mode is fully analogous to the FP rings.

Let us introduce now the cavity order, an essential quantity in the following. Resonances of the Airy function are 2π-periodic with respect to 2ϕ and hence are also periodic with respect to $k_z = k \cos\theta$. Resonances may thus be consecutively numbered 1, 2, 3, $\cdots$. For a given wavelength λ in the source spectrum, let us denote k_o the associated wavevector. The number of resonances is limited since $2\phi \leq 2k_o L$, and $2\phi = 2k_o L$ at normal incidence $\theta = 0$. The cavity order m_c is the number of resonances, giving $m_c = \text{integer}[2\phi(\theta = 0)/2\pi] = \text{integer}[2nL/\lambda]$ [see (T3)]. As a consequence of $2\phi = 2k_o L \cos\theta$, there are m_c resonant angles θ_i with equally spaced $\cos\theta_i$. We denote here θ_o the closest to normal of these resonant angles, for which we have

$$2\phi(\theta_o) = 2\pi m_c = 2k_o \cos\theta_o L. \quad (6)$$

Among θ_i's, resonant angles larger than θ_c are those of truly guided modes (without mirror phase shifts), whereas resonances with angles smaller than θ_c (if at all), being coupled to the continuum of modes propagating in the vacuum, are spread over a finite angular width related to the cavity finesse F. It is only in the $R_1 R_2 \to 1$ limit ($F \to \infty$) that these modes can rigorously be considered as discrete.

For more complex cavities with, e.g., distributed mirrors (see Section II-F), the most meaningful measure of cavity order is indeed how fast 2ϕ changes with angle θ (as well as wavevector k or frequency).

For further analysis, the scheme of Fig. 3 in k_x–k_z plane is useful. Here, the z axis is normal to the cavity. A monochromatic source defines a quarter-circle of radius $k = k_o$ (spectral linewidth would be accounted for by replacing the circle by an annulus). The source is taken here as isotropic, unlike real dipoles. To quantify light extraction, we use the vertical axis: the identity $d\Omega = 2\pi \sin\theta \, d\theta = 2\pi \, d(\cos\theta)$ tells us that the angle $d\theta$ subtends a solid angle $d\Omega$ given within a constant factor $(2\pi/k_o)$ by the z projection of the elemental arc $k_o \, d\theta$. To further account for the FP resonances (dropping the slowly varying antinode factor for simplicity), we thus plot as a function of k_z the Airy function of (4) as indicated, peaking when $2\phi \equiv 2\pi$ (i.e., $k_z \equiv \pi/L$). Light emission within $d\theta$ is

TABLE I
BASIC EQUATIONS FOR AN FP CAVITY AND ITS MODES IN A SCALAR VIEW; LAST COLUMN: BRIEF EQUATION DESCRIPTION

Equation	N°	Comments
$\text{Airy} = \dfrac{T_1}{\|1 - r_1 r_2 e^{2i\phi}\|^2}$ and $2\phi = 2kL\cos\theta,\quad k = n\dfrac{\omega}{c}$	(T1)	Airy factor, round-trip phase, and wavevector versus pulsation
$2kL\cos\theta = \dfrac{4\pi}{\lambda}L\cos\theta = 2m\pi,\quad m \le m_c$	(T2)	Dispersion relation (internal angle)
$m_c = \text{Int}\left(\dfrac{2nL}{\lambda}\right) = \text{Int}\left(\dfrac{kL}{\pi}\right)$	(T3)	Cavity order (within a half-integer for mirror phase)
$2nL\cos\theta = m\lambda$	(T4)	Mode wavelength versus internal angle
$\dfrac{d\lambda}{d\theta} = \dfrac{-2nL\sin\theta}{m}$	(T5)	Derivative of above relation
$\Delta k_z = \dfrac{\pi}{L}$	(T6)	Mode spacing
$\Delta\lambda = \dfrac{2nL\cos\theta}{m(m+1)}$	(T7)	Next mode wavelength $\lambda_m - \lambda_{m+1}$
$\text{Airy} = \dfrac{T_1}{(1 - r_1 r_2)^2\left(1 + \dfrac{2r_1 r_2}{(1 - r_1 r_2)^2}(1 - \cos 2\phi)\right)}$	(T8)	Airy factor with normalized denominator
$2\phi = 2\pi m_c \dfrac{\cos\theta}{\cos\theta_o}\dfrac{k}{k_o} \approx 2\pi m_c\left(1 - \dfrac{1}{2}(\theta_2 - \theta_o^2) + s\right),\quad s = \dfrac{k - k_o}{k_o}$	(T9a)	Phase expansion and definition of relative spectral shift s
$\sin^2\phi \approx \dfrac{1}{4}\left(\pi m_c(\theta^2 - \theta_o^2 + 2s)\right)^2$	(T9b)	Approximate squared sine of phase
$F = \dfrac{\pi(R_1 R_2)^{1/4}}{1 - \sqrt{R_1 R_2}} = \dfrac{\pi\sqrt{r_1 r_2}}{1 - r_1 r_2}$	(T9c)	Finesse (high reflectivity approximation)
$F \approx \dfrac{2\pi}{1 - R_1},\quad R_2 = 1,\ R_1 \to 1$	(T9d)	Finesse trend for perfect back mirror
$\text{Airy} \approx \dfrac{T_1}{(1 - r_1 r_2)^2(1 + F^2 m_c^2(\theta^2 - \theta_o^2 + 2s)^2)}$	(T9e)	Airy factor expansion as a Lorentzian

basically proportional to the product Airy $\times d\Omega$. Light that may be extracted is just that emitted at angles θ smaller than θ_c. Thus, extracted light is measured by the area under the Airy function between boundaries $k_z = k_o$ and $k_z = k_o\cos\theta_c$, shaded in Fig. 3(a). This range of k_z from $k_o\cos\theta_c$ to k_o will be termed below the "escape window." Note that the relative width of this window compared to k_o is $(1 - \cos\theta_c) \approx 1/2n^2$.

At this stage, two questions can be simply answered. 1) How small should a cavity be to have a single resonance throughout the escape cone? 2) What is the benefit in terms of extraction and brightness? The second question may be answered from a mode-counting argument by remarking that, in the $R_2 R_1 \to 1$ limit where the Airy function is a Dirac comb, all resonances gather equal fractions of emission as far as the Airy function is concerned. Although this does not hold for the antinode factor ζ, it does not affect mode-counting arguments by more than a factor of two: namely, a source located at the center of a symmetric cavity couples only to symmetric modes. The

| Equation	N°	Comments
$$\frac{\Delta\lambda}{\lambda} \approx \frac{\Delta k}{k} = \frac{\Delta\omega}{\omega} = S = \frac{1}{\pi m_c}\frac{1-\sqrt{R_1 R_2}}{(R_1 R_2)^{1/4}} = \frac{1}{Fm_c}$$	(T10)	Relative spectral width at half-maximum of Airy factor
$$\theta_{\mathrm{fwhm}}^2 - \theta_o^2 = \frac{1}{\pi m_c}\frac{1-\sqrt{R_1 R_2}}{(R_1 R_2)^{1/4}} = \frac{1}{Fm_c}$$	(T11)	Half-maximum internal angles from Lorentzian expansion
$$\Delta\theta = 1/(Fm_c\theta_o), \quad \Delta\theta < \theta_o$$	(T12a)	Internal angle (off-axis)
$$\Delta\Omega = 2\pi/Fm_c, \quad \text{idem}$$	(T12b)	Internal solid angle (idem)
$$\theta_{\mathrm{fwhm}} = \sqrt{1/Fm_c}, \quad \theta_o \ll \theta_{\mathrm{fwhm}}$$	(T13a)	Internal angle (on-axis lobe, $\theta_o = 0$)
$$\Delta\Omega = \pi/Fm_c, \quad \text{idem}$$	(T13b)	Internal solid angle
$$\Delta\Omega_{\mathrm{out}} = (2\pi/Fm_c)n^2(\cos\theta_{\mathrm{out}})^{-1} \approx 2\sqrt{2}((\pi/Fm_c)n^2), \quad \Delta\theta < \theta_o = \frac{1}{\sqrt{2}n}$$	(T14)	Outside solid angle, 45° off-axis resonance
$$\Delta\Omega_{\mathrm{out}} \approx (\pi/Fm_c)n^2, \quad \theta_o \ll \theta_{\mathrm{fwhm}}$$	(T15)	Outside solid angle (on-axis lobe)
$$a = \frac{\lambda}{4n}\sqrt{Fm_c} = \sqrt{\frac{\pi\lambda L}{8n}\frac{(R_1 R_2)^{1/4}}{1-\sqrt{R_1 R_2}}}$$	(T16)	Mode radius (on-axis lobe)
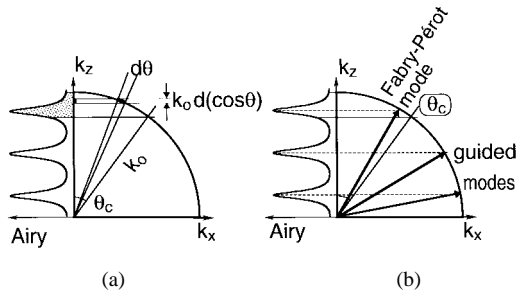
Fig. 3. Plot in k-space depicting cavity modes, critical angle, monochromatic emission, and the Airy function. (a) Emission from the microcavity is essentially proportional to the shaded area below the Airy function. (b) At angles above θ_c, there is one guided mode at each Airy peak, at a discrete angle. The FP mode is the single outgoing one, if at all, in a microcavity.

equality of mode weights is also easily derived in quantum mechanics using the product of single-photon field amplitude, whose only space-averaged square is considered here, with the density of photon final states, involving group velocity of guided modes (see below and [46] about mode weights). In our approximate approach, Fig. 3 still accounts for the two most important features of outside and guided modes: their about-equally-spaced $\cos\theta$ values and their equal coupling weights within an antinode factor correction; it is only misleading in

suggesting some finite angular spread for guided modes instead of Dirac peaks of equivalent area.

With modes equally coupled, it becomes obvious that extraction in a cavity with sharp well-separated resonances is the ratio $\eta = $ [number of outside modes/total number of modes], or the same ratio for odd modes in the centered source case. In the large-cavity limit, as illustrated in Fig. 4(a), this ratio tends toward the ratio of solid angles $\Omega_c/(2\pi) = 1 - \cos\theta_c$ because the $\cos\theta_i$'s are equally spaced from 1 to 0 and thus extraction tends toward $\eta \approx 1/2n^2$, as in the far-mirror case above due to the naive power reflection at the back mirror.

To take advantage of microcavity effects, there should not be many modes but only a few, and only one going out [Fig. 4(b)], a situation where the extraction is straightforwardly

$$\eta = \frac{1}{m_c}. \tag{7}$$

A direct approach from (4) in the same limit amounts to the sum of a Lorentzian function as a limit form of the Airy factor and also yields $1/m_c$.

For those concerned at this stage with the role of the antinode factor ζ, we temporarily reintroduce it still in the mode-counting limit (infinitely sharp resonances) and get a slightly more general result: for each resonance labeled
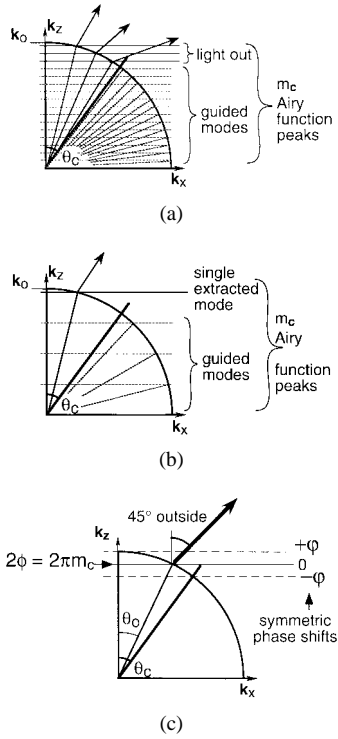
(a)

(b)

(c)

Fig. 4. (a) Large-cavity limit: many modes are extracted but the ratio of extracted to guided modes tends toward the no-cavity far-mirror extraction ratio. (b) Microcavity regime: one out of a small number of modes is extracted. (c) Centering the Airy peak in the k_z escape window gives a 45° outside angle.

$i = 1, 2, \cdots, m_c$, the more exact mode weight is given by its antinode factor ζ_i which accounts for the source position into the profile of the ith mode. Then the extraction η is the ratio $[(\sum \zeta_i$ of extracted modes $)/(\sum \zeta_i$ of all modes$)]$, which becomes $\zeta/(\sum \zeta_i$ of all modes$)$ for a single extracted mode of antinode factor ζ. It can be shown that except for $m_c = 1$, the ζ_i's average value is generally close to unity, hence in (7) $\eta = 1/m_c$ for $\zeta = 1$. In the following, we restore the assumption $\zeta = 1$. A full discussion is needed to take into account polarizations, dipole orientations, lifetime modifications, etc. (see [46] and also [17], [38], [40], [52], [53]).

Let us now discuss extraction enhancement taking as a reference the far-mirror case in which the back mirror just reflects emitted power toward $z > 0$ without any interference effect so that the extraction is $\eta = 1/2n^2$. Clearly, from (7), a cavity may increase η above the value $\eta = 1/2n^2$ only if its order m_c is smaller than $2n^2$. Thus, the threshold

$$m_c = 2n^2 \qquad (8)$$

defines the onset of the extraction-wise microcavity regime. We may also answer the first question: the limit to have a single resonance in the escape cone is when the round-trip phase exactly spans 2π on the $0 \rightarrow \theta_c$ domain, much in the same way as $2\phi'$ for the close-mirror case. Assuming $\cos \theta_o \approx 1$, we have

$$2\pi = 2\phi(\theta = 0) - 2\phi(\theta_c) \approx 2\pi m_c(1 - \cos \theta_c) \approx 2\pi(m_c/2n^2)$$
$$(9)$$

and we obtain the same threshold for microcavity regime $m_c \leq 2n^2$, not surprisingly. In this regime, modes have to be treated individually for all properties of the cavity, and chiefly angle- or spectrum-averaged ones such as extraction efficiency or brightness. Above this regime starts a "meso-cavity" regime where a small number of outgoing modes still leave pronounced directional features in the emission diagram rather than a smooth Lambertian law. Defining the upper bound $m_c^{\max}$ of this meso-cavity situation is, however, strongly dependent on more cavity parameters, not just the index. We shall denote in the following $v = m_c/n^2$, a ratio that will appear in many formulas.

Coming back to a single extracted mode, let us discuss the exact resonance location for optimal extraction. To obtain the largest area under the Airy function, the peak resonant angle θ_o should be centered into the escape window by symmetrizing phases at window edges $2\phi(\theta = 0)$ and $2\phi(\theta = \theta_c)$ and leaving $\cos \theta_o$ halfway between 1 and $\cos \theta_c \approx 1 - 1/2n^2$

$$\cos \theta_o = 1 - \frac{1}{4n^2}. \qquad (10)$$

At first-order $\theta_o \approx 1/\sqrt{2}n$. Then, 2ϕ evolves at most from $2\pi m_c + \pi \equiv \pi$ at normal incidence to $2\pi m_c - \pi \equiv \pi$ at grazing incidence, yielding antiresonances at escape cone edges [Fig 4(c)] and a 45° peak outside angle; the cavity is "detuned" to oblique angles to take advantage of the increase in the solid angle, but qualitatively not above about 45°: further gain in extraction is balanced toward grazing outside incidence angles by the decreased "solid angle transfer ratio" $d\Omega_{\mathrm{int}}/d\Omega_{\mathrm{out}} = (n_{\mathrm{out}}/n)^2 \cos \theta_{\mathrm{out}}/\cos \theta$, resulting from Snell's law cusped evolution at grazing incidence which dictates that external power in the largest outside angles has to be fed from vanishing internal solid angles.

We need in the following an approximate analytical expression of the Airy denominator, denoted D, around its (k_o, θ_o) resonance which we briefly detail here. Starting from

$$|1 - r_1 r_2 e^{2i\phi}|^2 = (1 - r_1 r_2)^2 \left(1 + \frac{2r_1 r_2}{(1 - r_1 r_2)^2}(1 - \cos 2\phi) \right)$$
$$(11)$$

and using in (5) a development of $\cos \theta / \cos \theta_o$ and k/k_o, we have at first-order

$$2\phi \approx 2\pi m_c \left(1 + \frac{1}{2}(\theta^2 - \theta_o^2) + \frac{(k - k_o)}{k_o} \right) \qquad (12)$$

and since $2\pi m_c$ is a multiple of 2π, we have when taking the cosine

$$(1 - \cos 2\phi) \approx \tfrac{1}{2} \left[\pi m_c(\theta^2 - \theta_0^2) + 2s \right]^2 \qquad (13)$$

where $s = (k - k_o)/k_o$ denotes the relative spectral shift. Taking (13) into (11), the Airy factor is transformed into the Lorentzian form (T8) or (T9b).

Integration of these formulas over angle and spectrum give the main trends to extraction evolution with microcavity

parameters. In Section II-C, a simple practical working point is determined to reach most attainable extraction in a lossless case.

C. Practical Working Point for Lossless FP Cavities

The main scope of this section is to discuss intrinsic reasons why optimizing light extraction requires only moderate reflectivities and finesses. Two extrinsic reasons to be discussed later are: 1) losses, preventing a large number of round-trips in the cavity and 2) the nonzero natural linewidth which leads to a situation where improving extraction efficiency at some wavelengths only occurs at the expense of other ones, resulting in an efficient spectrally-narrowed source but with no wavelength-integrated extraction enhancement (see Section II-E for details). In general, highly resonant cavities could even lead to an unwanted angle dependence of perceived color for display applications.

But even without such considerations, when the effort for maximizing extraction is balanced with the expense of higher reflectivity mirrors, a "working point" appears beyond which increased reflectivity hardly translates into a sizeable increase of extraction. Although it may be satisfactory to extract a peaked spectrum or a very narrow cone from an otherwise broad or Lambertian emitter, we will show that the highly reflective mirrors needed for this purpose bring only minute improvements to extraction, if at all, switching to a detrimental effect when going beyond extrinsic limits such as those of lossy cavities (Section II-D).

For simplicity, we consider here R_2 as unity, which leads to an upper estimate for the front reflectivity R_1 which is the only variable. This study of a "working point" to get light in the natural escape cone will be easily extended to smaller aperture requirements as those for coupling to fibers ($\Delta\Omega < 2\pi sr$ outside, Section II-G).

Our basic argument is as follows. Once a single Airy peak has been reasonably squeezed to fit well into the escape window $[k_o \cos\theta_c, k_o]$, increased reflectivity only marginally translates into increased extraction.

On the way to increased extraction via increased R_1, we want to know when most of the improvement from η toward η_{max} is reached, say 80% or 90%, to trade far easier fabrication requirements with minute "imperfections." Referring to Figs. 3–4, increasing R_1 amounts to concentrate emission of a k_z slice of extent $\Delta k_z = k_o/m_c$ into each mode. As a minimum requirement, we want this emission to be concentrated in a window of width $\delta k_z = k_o/2n^2$. Hence, the required finesse is of the order of $\Delta k_z/\delta k_z = 2n^2/m_c$, increasing for larger indices (smaller final window) and for smaller cavity orders (larger initial k_z slice).

These trends are illustrated in Fig. 5 presenting extraction η as a function of R_1 ($R_2 = 1$) for extreme indices ($n = 1.7, 3.7$) and cavity orders $m_c = 1$ [Fig. 5(a)] and $m_c = 2$ [Fig. 5(b)]. Even for the "worst case" $m_c = 1, n = 3.7$, reflectivities of 90%–95% are enough to achieve 80%–90% of η_{max}. For less stringent cases, say $m_c = 2$ (hence $\eta_{max} = 1/2 = 50\%$) and $n = 1.7$, η reaches 40%, i.e., 80% of η_{max} using R_1 as low as 65%, a very moderately resonant cavity. For still larger cavities, close to the limit $m_c = n^2$, most of
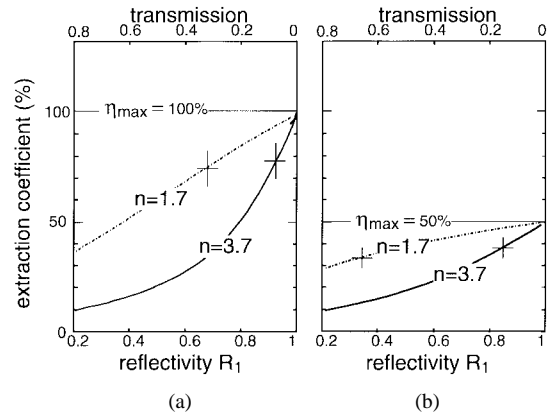

Fig. 5. (a) Extraction as a function of top mirror reflectivity R_1 for indices $n = 1.7$ (dash–dotted lines) and $n = 3.7$ (solid lines) for cavity order 1. (b) The same for cavity order 2; crosses are drawn at $R_1 = 1 - m_c/n^2$.

the improvement is gained for reflectivities below 50% with a flat trend beyond.

A more general rule is obtained by imposing that the Airy factor has to be at the edges $\theta = 0$ and $\theta = \theta_c$ of the escape cone about ten times smaller than its peak, because then there is little light lost between the extracted Airy peak and the next one. Noting that the Airy denominator [(T8)] increases at $\theta = 0$ and $\theta = \theta_c$ from its resonance minimum D_{min} to a value approximately given by

$$D(\theta = 0) = D(\theta = \theta_c)$$
$$\approx D_{min}\left[1 + \frac{r_1}{(1-r_1)^2} \times \left(\frac{\pi m_c}{2n^2}\right)^2\right] \quad (14)$$

most of the concentration in the resonant mode is achieved when the second factor is about 10. This translates into $T_1^{crit} \approx m_c/n^2 = v$ as a safe practical "working point" and

$$R_1^{crit} = 1 - \frac{m_c}{n^2} = 1 - v \quad (15)$$

a value generally below 90%, in agreement with recent microcavity LED's in particular studies [9], [11], [18]–[20], [22]–[25], [32]. It is easy to show that such a reflectivity gives $\eta/\eta_{max} \approx [2\arctan(\pi)/\pi] \sim 80\%$, leaving little room for improvements. The validity of this rule of thumb is of course a matter of application. Notice also that the extracted mode solid angle (at half-maximum) for this peculiar reflectivity value is $\Delta\Omega^{crit} \approx 1/n^2$ in the solid and thus about 1 sterad in air (see Table I). Beyond this point, directionality may increase but not extraction because the main lobe is only more squeezed but does not carry more power.

D. Effect of Losses

When losses are present, interferences in the FP cavity are diminished through the diminished reflectivities and/or the absorption in the cavity itself. Since all loss mechanisms eventually attenuate the round-trip amplitude, their effect for extraction can be cast in a unique cause, for example, only a back mirror of reflectivity $R_2 < 1$ and a lossless cavity, as we shall do here. Losses per pass are thus $1 - R_2$. Effects neglected in doing so are those depending on the peculiar position of the absorber with respect to the profile of the relevant modes. This
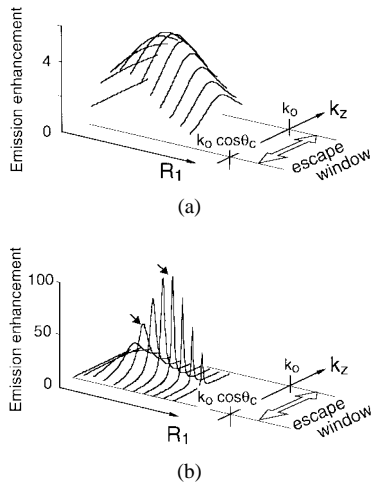
Fig. 6. Emission enhancement for k_z value in the escape window for (a) large losses and (b) small losses for variable R_1. In this case, maximum extraction (left arrow) occurs at a much lower reflectivity than maximum resonant intensity (right arrow). Successive reflectivities R_1 are, for example, 60%, 80%, 90%, 95%, etc, i.e., $1 - R_1$ forms a geometric series of ratio 2.

provision is similar to the one made about antinode factors, now applied to localized absorbers.

In this view, one obtains for the Airy function as a function of k_z but restricted to the escape window $[k_o \cos \theta_c, k_o]$ the graphs of Fig. 6, depicting how the Airy peak builds up, when front reflectivity R_1 is increased at given losses $1 - R_2$. Two values of losses are chosen in this example: $R_2 \ll R_1^{\text{crit}}$ in Fig. 6(a) (large losses) and $R_2 \gg R_1^{\text{crit}}$ in Fig. 6(b) (small losses). In both cases, the resonant Airy peak value goes through a maximum when R_1 exceeds R_2, the maximum at resonance thus corresponding to equal power flows at the two mirrors. This is the obvious result that "exit losses" at the front mirror ($T_1 = 1 - R_1$) should be larger than dissipative losses ($1 - R_2$) to collect more power on the front side, i.e. $R_1 \leq R_2$ as a basic requirement [16].

It clearly appears in Fig. 6(a) that the Airy peak remains so broad for large losses that the extraction efficiency, i.e., the area below the curves, closely follows the evolution of emitted intensity at the resonant angle, peaking at about the same condition $R_1 \approx R_2$.

The behavior of extraction efficiency at low losses is obviously different in Fig. 6(b) where the Airy peak gets sharp enough to largely fit into the escape window as soon as $R_1 \approx R_1^{\text{crit}}$, and well before the emitted intensity at exact resonance reaches its own maximum ($R_1 = R_2$). This implies that the peak area now diminishes far before this maximum: since the tails play here a negligible role, the peak relative sharpening is not compensated by a sufficient increase of its height. Hence, optimal extraction is attained for T_1 ("exit losses") much larger than the losses $1 - R_2$, unlike the case of strong losses. In other words, concentrating photons into a sharply resonant mode rapidly demands so many round trips that cumulated losses degrade extraction. Optimal extraction then corresponds to a tradeoff between mode sharpening which diminishes the fraction lost in mode tails outside the escape window, and mode spreading which diminishes the number of round trips and associated losses.

A quantitative account of these trends requires a few calculations given in Appendix A as well as the crossover outlined above. The space of parameters can be reduced to the $(1 - R_2, m_c/n^2) \equiv (\text{loss}, v)$ plane under some assumptions. The enhancement of the extraction coefficient over the bare case is numerically optimized resulting into two maps giving: 1) the optimized front reflectivity R_1 in the $(\text{loss}, v) \equiv (1 - R_2, m_c/n^2)$ plane and 2) the optimized extraction enhancement factor. In a large part of the parameter plane, analytical optimization could be also performed. Finally, the tradeoff between cavity order and losses arising when choosing distributed reflectors rather than metals is detailed in Section II-F.

Summarizing this subsection and the previous one, in the presence of losses, the basic design rule becomes $R_1 = \min(R_1^{\text{crit}}, R_1^{\text{loss}})$, the latter stemming from the above optimization. Of course, in the vanishing loss limit, the large reflectivities of, e.g., >99% as those needed for the much-studied vertical (micro)-cavity surface-emitting lasers (VCSEL's) are in principle the best, since without losses more resonance always brings more light into the favored mode, saturating at the value given by mode counting ($\eta = 1/m_c$). But this limit, dictated by the specific VCSEL's need for strong optical feedback, is less relevant for extraction purpose for which the design rule we propose implies reflectivities below 90%.

We have so far been concerned with a quasi-monochromatic approach. Introducing the effect of spectral linewidth is now appropriate.

E. Impact of Spectral Width of Sources, Brightness, and Directionality Issues

Dealing in k terms with sources of finite spectral width, we denote the relative width $S = \Delta k/k_o$ for natural width at half maximum Δk centered at k_o, and $s = (k - k_o)/k_o = \delta k/k_o$ the relative shift of a particular frequency. We introduce here the brightness (or radiance), which is the wavelength-integrated emitted power per unit area and unit solid angle. In microcavities, brightness and directionality are closely related due to the unavoidable angle-wavelength dispersion of cavity modes [11], [15], [16], [28], [33]. This dispersion follows from (6), $kL \cos \theta = 2\pi m_c$, which is conveniently written for the extracted mode as

$$k = k_o \cos \theta_o / \cos \theta, \quad \lambda = \lambda_o \cos \theta / \cos \theta_o \qquad (16)$$

at resonance. However, due to the partial mirror reflectivities and finite finesses, each wavelength is emitted in a lobe with an internal angular width given by (T12). This spread is denoted here $\Delta \theta_{\text{mono}}$ as it has a monochromatic origin. On the other hand, it follows from (16) that the finite spectral width S translates into an angular spread $\Delta \theta_{\text{poly}}$. We give in Appendix B the detail of these quantities and the various regimes that occur depending on S and on the cavity characteristics; we present here the main conclusions concerning brightness enhancement denoted B, directionality and extraction.

In a perfectly monochromatic case and without losses, the brightness of the resonant lobe extracted from a microcavity normalized to a unit emitter is essentially the ratio of extracted
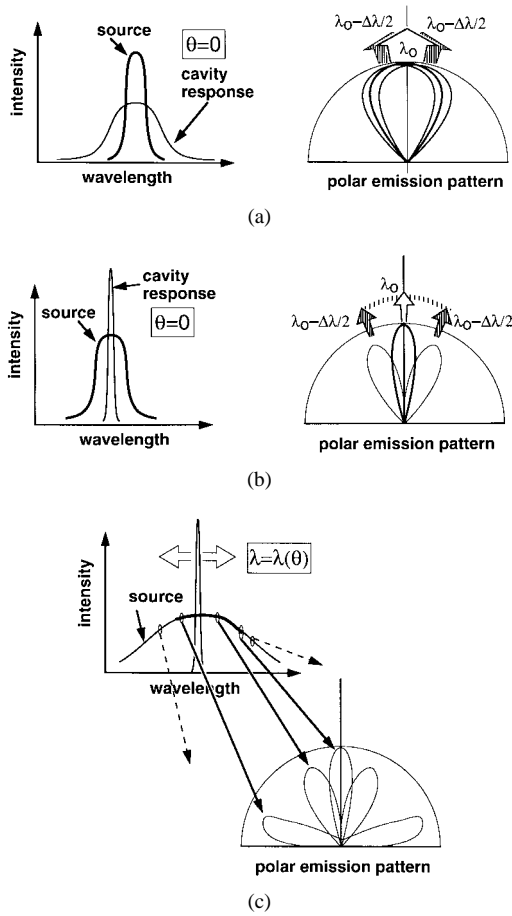
Fig. 7. (a) Cavity resonance larger than the source natural spectral width, no directionality. (b) Cavity resonance narrower than the source natural spectral width, the different wavelengths are emitted into different directions. (c) The same as (b) but for very large spectral width: extreme wavelengths cannot be extracted.

power, at most $1/m_c$, by the lobe solid angle, which is well approximated by $2\pi/Fm_c$ [(T12b) of Table I] for the internal lobe [(T12b)]. Compared to the no-cavity normalized value $1/4\pi$, this yields a brightness enhancement $B \approx 2F$ (as argued by [47] some time ago). External brightnesses are in the same ratio as internal ones and need not be explained here. This monochromatic enhancement has no intrinsic upper limit, unlike extraction, which was argued to saturate for finesses above the moderate one associated with R_1^{crit}.

However, taking spectral width into account, brightness may follow the increase in finesse only if $\Delta\theta_{\mathrm{mono}} \gg \Delta\theta_{\mathrm{poly}}$: viewing each mode as a ring, as in a classical FP interferometer, this condition ensures that each FP ring is still broader than the chromatic angular separation, and only the ring edges experience some chromatic effects [see Fig. 7(a)]. Conversely, if $\Delta\theta_{\mathrm{mono}} \ll \Delta\theta_{\mathrm{poly}}$, for large finesses, rings of the different emitted wavelengths are well separated [Fig. 7(b)]. In this limit, brightness, a wavelength-integrated quantity, cannot increase anymore since each elemental angle $d\theta$ is uniquely coupled to a given spectral slice $dk = d\lambda/\lambda^2$ according to (16). High brightness is thus best achieved with a very monochromatic source $(S \to 0)$ and a very high-finesse cavity, and inevitably translates into a highly directional emission pattern.

An overall rule for both regimes is

$$B\Delta\Omega m_c \approx 4\pi \qquad (17)$$

where B is the brightness enhancement over the no-cavity case, and $\Delta\Omega = \max(\Delta\Omega_{\mathrm{mono}}, \Delta\Omega_{\mathrm{poly}})$ is the largest of the two solid angles with obvious notations. This originates in the fact that the cavity distributes the light previously emitted over 4π sterad over m_c Airy peaks (or, in other words, m_c FP rings) within a solid angle $\Delta\Omega$ for each. Brightness increases just as directionality, until a saturation is reached due to the finite spectral width S, in which case directionality saturates to $\Delta\Omega_{\mathrm{poly}}$. In this regime $(\Delta\theta_{\mathrm{mono}} \ll \Delta\theta_{\mathrm{poly}})$, if light is detected only within a infinitely small solid angle, e.g., very close to normal incidence, spectral narrowing takes place: it is easy to find that the apparent spectral width becomes $S(\Delta\theta_{\mathrm{mono}}/\Delta\theta_{\mathrm{poly}}) \ll S$. This is, understandably, one of the most popular microcavity effects on spontaneous emission (refs), useful in cases where spectral narrowing is needed, but not leading to wavelength-integrated extraction efficiency, being even detrimental in the presence of losses.

In deriving (17) above, it was assumed that all wavelengths within the spectral width S could resonantly escape at some angle. This is impossible, however, if S exceeds a limit spectral width $S_{\mathrm{esc}} = 1/2n^2$, because the resonant mode is either cut-off on the small k (large wavelength) side or resonant at angles above the critical angle on the large k (short wavelength) side [Fig. 7(c)]. Above the limit $S = S_{\mathrm{esc}}$, we can crudely neglect the tails of all modes with such nonescaping resonances and insert a factor (S/S_{esc}) in the left-hand side of (17). Brightness thus scales like S_{esc}/S in this regime, a diminished part of emitted power being resonantly extracted when S increases.

Extraction efficiency follows the same rule: extraction enhancement up to the best value $1/m_c$ of (7) holds in the regime $S \ll S_{\mathrm{esc}}$, and conversely, extraction is diminished by a factor of at least (S_{esc}/S) in the large spectral width regime $S \gg S_{\mathrm{esc}}$. In this case, we find in Appendix B a critical reflectivity

$$R_1^{\mathrm{sp,crit}} = 1 - 2m_c S \qquad (18)$$

which is an analog of R_1^{crit}: beyond this reflectivity value, there are only marginal gains for extraction. Notice that escaping to epoxy rather than air brings a substantial improvement for the many materials featuring linewidth S in the 5%–10% range by pushing away the limit set by S_{esc}: S_{esc} in epoxy is 2.25 times larger than in air (the squared epoxy index) and falls in the useful 10% range for typical semiconductor indices slightly above $n = 3$, instead of just 5% in air.

The overall trends exposed in this section are summarized in Fig. 8 reporting the main trends of extraction, brightness, and directionality in a characteristic example that can be easily generalized $(n = \sqrt{10} = 3.16$ and $m_c = 2)$. The ordinate is the spectral width S while the abcissa was chosen here as the top mirror reflectivity R_1 but can easily be interpreted in terms of the lobe internal solid angle $\Delta\Omega = \Delta\Omega_{\mathrm{mono}}$ or the finesse $F = 2\pi/m_c\Delta\Omega_{\mathrm{mono}} = \pi/\Delta\Omega_{\mathrm{mono}}$. Trends for extraction efficiency are simple in the case $S < S_{\mathrm{esc}} = 5\%$
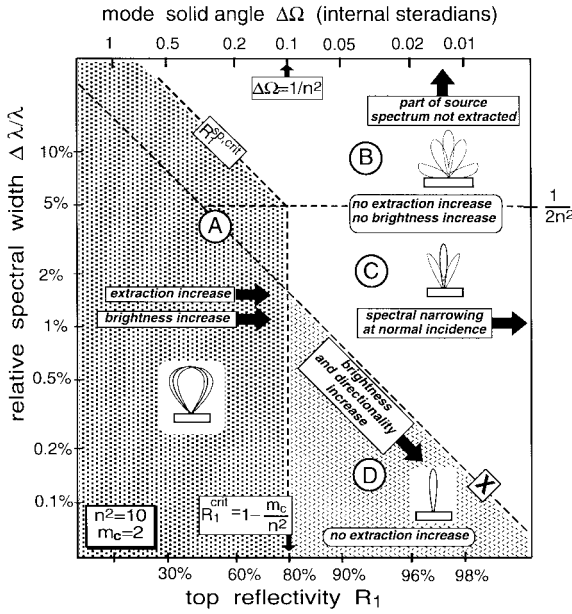
Fig. 8. Summary of the trends of extraction and brightness increases in the (reflectivity, spectral width) or $(\Delta\Omega, S)$ plane in the particular case $m_c = 2$ and $n^2 = 10$. In region A, both quantities increase. In regions B and C, none of them increase. In region D, only brightness increases. Above line X, spectral width causes more angular spread than does cavity finesse. Going from C to B prevents all wavelengths to be extracted ($S > S_{esc} = 1/2n^2$). The frontier between A and B is at $R_1^{sp,\,crit}$. The frontier between A and C is at $R_1 = R_1^{crit}$ and $\Delta\Omega = 1/n^2$.

here: there is an increase for reflectivities below R_1^{crit} in region A followed by a saturation when R_1 is above R_1^{crit}. But, if S exceeds $S_{esc} = 5\%$ (region B), saturation occurs at the lower reflectivity $R_1^{sp,crit} < R_1^{crit}$.

Trends for brightness improvement are different because angular integration is not required for this latter quantity. Hence brightness cannot increase when the monochromatic mode solid angle $\Delta\Omega_{mono}$ becomes smaller than the source-dependent but cavity-independent solid angle $\Delta\Omega_{poly}$. This cross-over between $\Delta\Omega_{poly}$ and $\Delta\Omega_{mono}$ occurs along the line labeled X, on the right of which brightness cannot increase. Thus brightness and directionality may further increase together only into region D (smaller spectral width at given R_1), where $\Delta\Omega_{poly} < \Delta\Omega_{mono}$. Conversely, if $\Delta\Omega_{poly} > \Delta\Omega_{mono}$ (region C, larger spectral width at given R_1), the cavity resonance is too monochromatic to accomodate all emitted wavelengths into $\Delta\Omega_{mono}$.

Thus, spectral narrowing occurs if a measurement is performed, for example, at normal incidence. A small part of region A, right of the crossover line X, follows the same trend. Finally, in region B, due to the large spectral width, not only is brightness saturated, but the whole outside emission in 2π sterad is truncated to the $\sim5\%$ maximum spectral width which can be resonantly extracted from a cavity of index $n = \sqrt{10} = 3.16$.

Eventually, for a general situation with both losses and non-negligible spectral width, the suggested design rule for optimal extraction is to take the smallest of the three reflectivities

$$R_1 = \min\left(R_1^{crit}, R_1^{sp,crit}, R_1^{loss}\right). \qquad (19)$$

F. Distributed Bragg Reflectors (DBR) Systems

Turning to realistic LED and emitter systems, DBR stacks made of alternate low-index (n_{lo})/high-index (n_{hi}) layers, denoted LHLH..., are often the only low-loss or simply feasible mirror solution [16], [18], [23], [32], [39], [44], [54]–[57]. Their key parameter is the relative index difference $\Delta n/n_{mid}$ where n_{mid} is the average DBR index [58]. Attainable Δn values are dictated by epitaxial or deposition constraints inherent to materials, notwithstanding conductance considerations. We briefly recall some DBR features before discussing how they degrade extraction due to their finite penetration length which increases the effective cavity order.

DBR mirrors capitalize on successive reflections at dielectric interfaces [50], [51], [59]–[61]: For quarter-wave-layer optical thicknesses, phases from such waves are separated by $\phi_c = 2\pi$ at their central (nominal) wavelength λ_B. A typical case is GaAs–AlAs ($n_{lo} = 2.9$, $n_{hi} = 3.5$ around $\lambda = 1\,\mu m$) with each normal reflection being only 1.2% in power but 11% ($\sim\Delta n/2n_{mid}$) in amplitude. To grossly approach unity reflectivity, about $n_{mid}/\Delta n$ reflections are needed, e.g., six pairs for our example. This suggests a penetration length of a few $\lambda/2$ per DBR mirrors, a quantity that will be detailed below in a DBR-bounded cavity and which will help us to still apply the above approach, but with an increased effective cavity order.

Departing from the central wavelength, an infinite DBR may still build up unit reflectivity across a so-called stopband. At stopband edges, the penetration length L_p diverges and photon states are standing waves with antinodes either in L or H layers, just like bonding and antibonding states in the tight binding model of periodic electron potentials [62], [63]. The relative stopband width is given to a very good approximation by the first Fourier component of index profile $n(z)$, $\Delta S/S = (2/\pi)(\Delta n/n_{mid})$ [59]–[61]. Beyond their stopbands, DBR's are no longer "mirrors" and allow propagative photon states often called leaky modes.

In a finite DBR consisting of p pairs sandwiched between any two media, schematically n_o/LHLH$\cdots$LHLH/n_s, reflectivity at stopband center reads [59], [60]

$$R = R(p) = \left(\frac{1 - \dfrac{n_s}{n_o}\left(\dfrac{n_{lo}}{n_{hi}}\right)^{2p}}{1 + \dfrac{n_s}{n_o}\left(\dfrac{n_{lo}}{n_{hi}}\right)^{2p}}\right)^2 \qquad (20)$$

when n_o is the incident medium. If the stopband center lies at oblique incidence, n_i's are to be replaced by e.g. $n_i \cos\theta_i$ in s-polarized case (TE) with obvious notations.

We now examine the role of penetration length and phase evolution on cavity order. We stated above that the most meaningful measure of cavity order is how fast the round-trip phase 2ϕ evolves with angle or wavevector. To emphasize this, we may write 2ϕ as follows:

$$2\phi = k\cos\theta L = (k/k_o)(\cos\theta/\cos\theta_o)(2k_o\cos\theta_o L)$$
$$= 2\pi m_c (k/k_o)(\cos\theta/\cos\theta_o). \qquad (21)$$

When compared to a localized mirror (metal, single interface) with a well-defined phase change determined by dielectric
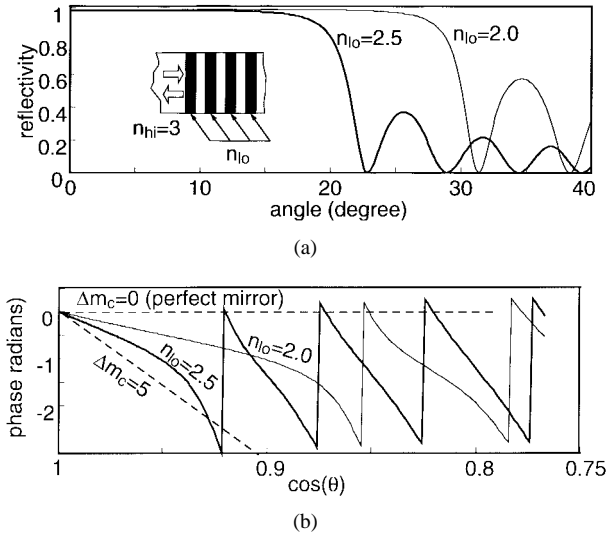
(a)

(b)

Fig. 9. (a) Power reflectivity of a DBR mirror with indices $n_{\mathrm{hi}} = 3$ and $n_{\mathrm{lo}} = 2.5$ or $n_{\mathrm{lo}} = 2$ as a function of the angle of incidence θ. (b) Phase of the reflectivity referenced at the first DBR layer (solid line) as a function of $\cos \theta$ showing the linear phase shift. Dashed lines: phase of a perfect mirror located at Δm_c half-wavelengths for $\Delta m_c = 0$ and 5.
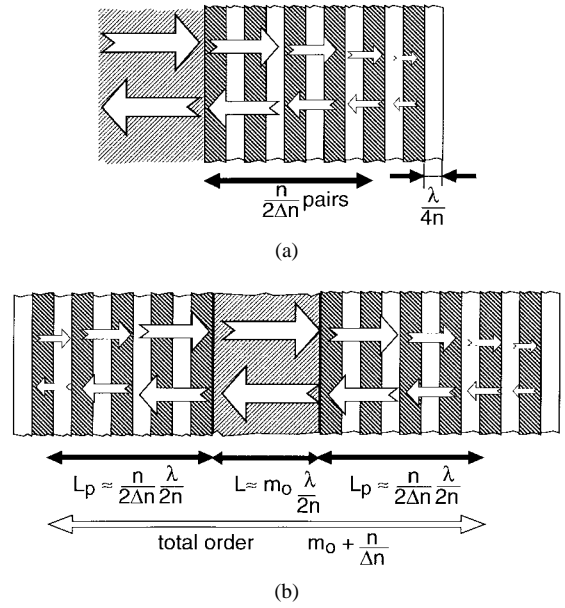

(a)

(b)

Fig. 10. (a) DBR mirror made of quarter-wave stacks and its penetration length, which adds to the bare cavity effective length, as pictured in (b) for a DBR/cavity/DBR system.

constants, a DBR mirror gives an angle and wavelength-dependent phase change at the first DBR interface with the cavity due to the phase changes of partial beams reflecting on successive interfaces. One thus has to add to the cavity phase change twice the phase changes at the DBR/mirror interfaces. These nonconstant phase changes then increase the bare cavity order $m_o = L/(\lambda/2n)$, a modification which in turn accounts for those of all the other interrelated properties of the cavity (quality factor, etc.).

We plotted in Fig. 9 the amplitude and phase of the complex reflectivity of (quasi-)infinite DBR's of various indexes contrasted at their nominal wavelength λ as a function of θ or $\cos \theta = k_z/k_o$. An angular stopband arises, as a natural counterpart of the spectral stopband [see (5)]. Across this angular stopband, it is seen that phase essentially evolves linearly, just as would do a wave reflecting at an imaginary perfect mirror placed at some location inside the DBR. This equivalent location is of course the penetration length L_p, which we may conveniently express in reduced units as $\Delta m_c = L_p/(\lambda/2n)$. In agreement with (5) and (6), a real mirror located at L_p would indeed give rise to a reflected phase $2\pi \Delta m_c \cos \theta$, as suggested by the dashed lines in Fig. 9(b). The penetration length is also illustrated in Fig. 10(a).

This discussion is made quantitative by the following formula for penetration length L_p [60]

$$L_p = \frac{\lambda}{2} \frac{n_{\mathrm{lo}}}{2n_{\mathrm{mid}}\Delta n} \qquad (22a)$$

$$\Delta m_c = \frac{n_{\mathrm{hi}}n_{\mathrm{lo}}}{2n_{\mathrm{mid}}\Delta n} \approx \frac{n}{2\Delta n} \qquad (22b)$$

and the order increase referenced to the high-index medium, which is within a factor of two inverse to the relative index step $\Delta n/n$. With (22), we account for the extraction trends of DBR-bounded cavities as follows.

Since cavity order essentially accounts for round-trip phase evolution either with detuning s or with angle $\cos \theta$ [(21)], to account for a symmetric cavity bounded by identical DBR's, as

pictured in Fig. 10(b), we add twice Δm_c to the "bare" cavity order m_o and obtain as the effective order of the compound cavity

$$m_c = m_o + 2\frac{n_{\mathrm{mid}}}{2\Delta n}\frac{n_{\mathrm{lo}}}{n_{\mathrm{mid}}} \approx m_o + \frac{n}{\Delta n}. \qquad (23)$$

We now examine important consequences of this larger order, firstly concerning the possibility of a microcavity at all, and secondly for adapting the above work to the DBR case, specifying in particular the number p of layer pairs needed at the critical working point (R_1^{crit}).

For vanishing index steps Δn, $m_o \ll n/\Delta n$ can be neglected, and the enlarged effective cavity order becomes $m_c \approx n/\Delta n$. It exceeds the threshold $m_c \approx 2n^2$ of the microcavity regime (single outgoing resonance) for $\Delta n < (2n)^{-1}$ in a symmetric case ($\Delta n < (4n)^{-1}$ in an asymmetric one for which $m_c \approx n/(2\Delta n)$). Fortunately, in the (In, Ga, Al)As testbed system [9], [18], [54], $\Delta n \approx 0.6 > 1/6$ and this system remains in the microcavity regime. It is not so clear cut for, e.g., InP- or II–VI-based systems where material constraints impose index steps of the order of $\Delta n = 0.2$ (see [46]).

We come back to the case of nonvanishing Δn. When a single mode escapes, we may rewrite the critical reflectivity formula (15) in terms of index step rather than cavity order

$$R_1^{\mathrm{crit}} \cong 1 - \frac{m_o}{n^2} - \frac{n_{\mathrm{lo}}}{n^2\Delta n} \approx 1 - \frac{m_o}{n^2} - \frac{1}{n\Delta n} \approx 1 - \frac{1}{n\Delta n} \qquad (24)$$

working with successive approximations of moderate index step and short bare cavity. We may also set up a simplified expression for the finite DBR reflectivity assuming similar indices of cavity and, e.g., DBR substrate

$$R(p) \approx 1 - 4\left(\frac{n - \Delta n}{n}\right)^{2p} = 1 - 4\left(1 - \frac{\Delta n}{n}\right)^{2p}$$

$$\approx 1 - 4\exp\left(-2p\frac{\Delta n}{n}\right). \qquad (25)$$

Matching $R(p)$ to R_1^{crit} gives the critical number p^{crit} of DBR pairs needed to gain most of the attainable extraction

$$p^{\text{crit}} \approx \frac{n}{2\Delta n} \log\left(4n\Delta n\right). \qquad (26)$$

This formula yields $p^{\text{crit}} = 6.2$ for the GaAs–AlAs system ($n = 3.5$, $\Delta n = 0.6$) in which a careful optimization gave a similar result [18], [19], $p^{\text{crit}} = 6$, actually as a result of compensations among a number of factors.

As for the back mirror in cavities bounded by two DBR mirrors, it should obviously be far more reflective than the top one to ensure escape on the front side. As a rule of thumb, when the number of pairs in the second mirror p_2 is twice p, we have $T_2 \approx T_1^2 \ll T_1$ which is in general sufficient.

A more profound modification arises when mirrors are asymmetric in nature: in many cases, one can take advantage from asymmetric DBR/cavity/metal structures, where one diminishes the cavity order from $m_c = m_o + n/\Delta n$ [(23)] to about $m_o + n/2\Delta n$, but at the expense of metal losses. The basic trend is that if m_o is small enough, we just halve the cavity order and expect ideally a doubled extraction $\eta_{\text{asym}} \approx 2\eta_{\text{sym}}$ if losses were absent.

Let us further the analysis and evaluate how much metal losses ($R_2 < 1$) are permitted before losing the advantage of reduced cavity order. We neglect the half-order (quarter wave) needed to accomodate the changed reflection sign of metals compared to dielectric cavity–DBR interfaces. We need also the constant extraction contours in the $(1 - R_2, v = m_c/n^2)$ plane of Fig. 12(b) given in Appendix A, and in particular their approximate constant slope of -1.6 in a large region. The upper value of metal losses to retain an extraction gain can be obtained by comparing the displacement in this plane to these constant extraction contours: one does not gain or lose extracted power if the variation Δv is accompanied by a loss variation such as $1.6 \times \Delta$ (losses) $= \Delta v$. Since we diminish m_c by $n/2\Delta n$, we have $\Delta v = -1/2n\Delta n$. Hence, the allowable round-trip losses due to the metal for overall gain using a metal instead of a DBR back mirror are

$$(1 - R_2)_{\text{max}} \approx \frac{|\Delta v|}{1.6} \approx \frac{1}{3.2n\Delta n}. \qquad (27)$$

This is a modest demand except for extremely contrasted DBR's, say $n\Delta n > 5$, which would call for limited round-trip losses not exceeding 5%. Thus, asymmetric structures probably offer the best compromise in many cases. Because it is impossible to grow epitaxial material on metal, DBR's on a substrate are preferred escape mirrors, whereas a thick gold or silver layer as the back mirror features low losses (it can also be deposited close enough to quantum wells, typically witin two or three half-wavelengths to ensure an antinode factor $\zeta = 2$ for all escape angles). One exception could be the rough or optically poor contacts based on some transition metals used as the easiest solution to fulfill electrical requirements and prevent, e.g., gold diffusion in highly injected structures. In this case, a hybrid metal–DBR mirror should probably be implemented. Assuming a reflective enough contact, and following for such an asymmetric DBR/cavity/metal structure the approach leading to (26) the diminished cavity order $m_c =$
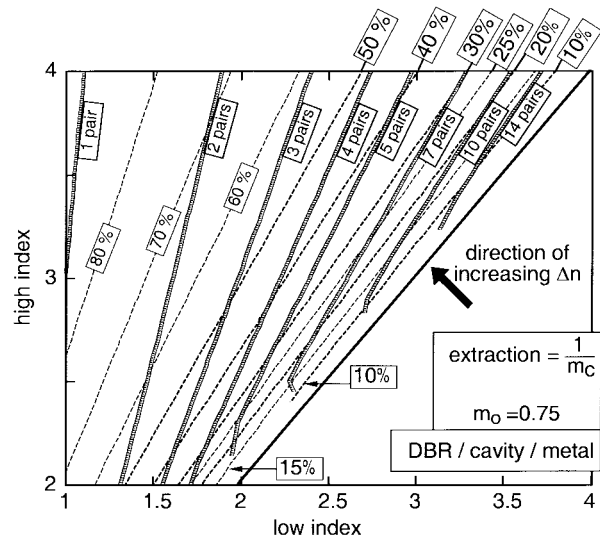

Fig. 11. Contour map of approximate extraction efficiency η (thinner dashed lines) and critical number of DBR pairs [according to (28), thicker lines] in the $(n_{\text{lo}}, n_{\text{hi}})$ plane for an asymmetric DBR/cavity/metal light-emitting structure: the source is monochromatic, the metal is lossless, the antinode factor is $\zeta = 1$, and the bare cavity order is $m_o = 0.75$ (see Fig. 3 of [Section II] for comparison). The index contrast Δn increases linearly above the $n_{\text{lo}} = n_{\text{hi}}$ line. Validity tends to break down for large Δn and $\eta > 50\%$.

$m_o + n/2\Delta n$ implies slightly more pairs in the remaining DBR mirror even if we do not neglect m_o

$$p^{\text{crit}} \approx \frac{n}{2\Delta n} \log\left(4n\Delta n \times \left(\frac{2n}{2m_o\Delta n + n}\right)\right). \qquad (28)$$

For $m_o = 2$, $n = 3.5$, $\Delta n = 0.6$ (GaAs–AlAs), we find $p^{\text{crit, asym}} = 7.4$ instead of $p^{\text{crit,sym}} = 6.2$, not a major change. In this system, limits for metal losses are as high as $(1 - R_2)_{\text{max}} \approx 17\%$, easily satisfied by noble metals. Without losses, the diminished cavity order ($m_c = m_o + n/2\Delta n$ instead of $m_o + n/\Delta n$) would translate into an extraction ($1/m_c$) increased from 11% to 20%. Additional enhancement factors [9], [18], [19], [22], [24] including, e.g., dipole orientation, photon recycling, etc., indeed resulted in 23% efficiency [23], [25] in such an asymmetric structure with a six-pair DBR on one side and a nonalloyed high-reflectivity metal contact on the other side.

To illustrate in a single figure the essential result of the analytical approach for an asymmetric DBR/cavity/metal structure [(7), (22b), and (28), namely], we present in Fig. 11 a map in the $(n_{\text{lo}}, n_{\text{hi}})$ plane showing the locus (contours) of given extraction efficiency $\eta = (1/m_c)$ and given value of p^{crit}, for a short bare cavity, $m_o = 0.75$. In this plane, there are of course no data below the line $n_{\text{lo}} = n_{\text{hi}}$. Above this line, the index contrast of the DBR linearly increases, and the cavity order diminishes leading to a rise in efficiency as well as a smaller number of DBR pairs needed to reach the critical reflectivity value (15). A similar map based on a more exact approach is presented in [46, Fig. 3]. Let us stress that this is a monochromatic lossless approach, thus a rather optimistic case. See Appendixes A and B for the effect of losses and spectral trends. Even without such detrimental factors, it is clear that the validity of this approximate scalar analysis breaks down in the large index contrast regime ($\Delta n > 1$) where there

are very few modes so that the exact knowledge of their antinode factors, for example, becomes crucial.

Finally, in the particular case of vanishing Δn, it may be advantageous in theory and in practice to shorten the DBR and replace its last layers by the natural DBR–air interface to build a shorter cavity. Given the large number of parameters, we only give here a hint on this case, assuming that the air–DBR reflectivity, typically 30%, is a given parameter: starting from the bare cavity bounded by air, one inserts DBR layers of small index contrast, thus enlarging the cavity. This increases both the reflectivity R_1 and the cavity order m_c, which in turn decreases R_1^{crit}. One should then self-consistently select the reflectivity which satisfies $R_1 = R_1^{\mathrm{crit}}$, the criterion of Section II-C, now seen as an implicit equation with the number of pairs p as a parameter.

In this section, we insisted on the enlarged cavity order to draw the main consequences for extraction. It is also interesting to restate the Airy function approach (Fig. 3) in the presence of DBR's which display large reflectivity only in their stopband. This is done in Appendix C where leaky modes allowed outside the stopband are discussed in this framework based on reflectivities (see Fig. 13). This also allows to give a hint on design rules for DBR-based cavities. The main conclusion of Appendix C is the importance of large index contrasts $\Delta n / n$ to diminish unwanted emission into leaky modes (see Fig. 14). It also gives hints on the spectral dependence of emission into leaky modes, on the role of leaky modes in hybrid DBR–metal cavities and on the role of guided modes of the bare cavity.

G. Dealing with Small Aperture Requirements

It is rather easy to now account for optimized coupling to some limited external angle denoted θ for simplicity ($\sin(\theta) =$ numerical aperture, n.a.) and solid angle $\Omega = 2\pi(1 - \cos\theta)$, typically 0.3–0.5 sterad for a multimode glass fiber [16], [32], [33], [53], 1–2 steradians for LED's embedded in focussing lens-shaped epoxy packages, etc. [2]. We just have to look at the round-trip phase variation from (14) and impose concentrating the resonance over a narrower angular region

$$\delta(2\phi) \approx \frac{\pi m_c}{2n^2}\sin^2\theta \qquad (29)$$

rather than just $\pi m_c / 2n^2$, now yielding

$$R_1^{\mathrm{crit}} = 1 - \frac{m_c}{n^2}\sin^2\theta \qquad (30a)$$

$$p^{\mathrm{crit}} \approx \frac{n}{2\Delta n}\log\left(\frac{4n\Delta n}{\sin^2\theta}\right) \qquad (30b)$$

for, respectively, a general case and the DBR–DBR configuration with negligible m_o. For example, to couple from a $\sim$50-μm-diameter LED to a $\sim$100-μm core fiber with $\sin\theta = 0.25$ n.a. ($\theta = 14°$), we get, for GaAs–AlAs, $p_{\mathrm{crit}} \approx 14.3$ pairs instead of 6.2 previously. For an intermediate case, $\sin\theta = 0.5$ n.a. ($\theta = 30°$), $p^{\mathrm{crit}} = 10.3$ pairs (four extra pairs per factor of two in aperture). Note that brightness trends of Section II-E still hold in their principle. Referring to Fig. 8, the vertical boundary between regions A and D lies at smaller solid angles $\Delta\Omega$, i.e., larger reflectivities and larger finesses, by a factor

$\sin^2\theta$. Also, the horizontal boundary between regions B and C lies at a smaller spectral linewidth, $S = 1/(2n^2\sin^2\theta)$. This indicates that very large brightness enhancements from microcavities coupled to fibers are expected for narrow sources with typically $S \leq 1\%$ (however a rare case, that could be realized at room temperature only in controlled quantum dot systems not well mastered yet): for such sources, the power of the whole resonant mode is fully coupled to the fiber at all emitted wavelengths, instead of the fraction $\sin^2\theta / 4n^2$ of the 4π solid angle from an isotropic source. The $\eta \approx 1/m_c$ extraction coefficient still holds for this monochromatic limit because the same extracted mode as above may be squeezed into a cone of smaller angle. The fiber-coupled power enhancement is thus in this case

$$\frac{\eta_{\mathrm{fiber}}}{\eta_{\mathrm{fiber,\,bare}}} = \frac{4n^2}{m_c\sin^2\theta} \qquad (31)$$

which exceeds one hundred for the optimistic example of Fig. 8 ($n^2 = 10$ and $m_c = 2$) and $\sin\theta \sim 0.25$. Losses tend to grow in this more resonant case, so that the number of parameters (indices, cavity order, losses, spectral width, aperture) require a separate study for more details [16], [21], [32].

III. Conclusion of the Approximate Approach

We gave an analytical account of the large potential held by planar microcavities for improving light extraction from large index emitting systems such as semiconductors ($n \sim 3$). We showed through the number of competing FP modes why a small cavity order $m_c \leq 2n^2$ is crucial in achieving enhanced extraction. The naive limit to the extraction coefficient is then found to be simply $\eta = 1/m_c$, where we purposely omitted the effects of antinode factor ζ, at most factors of two. Note also that lifetime effects play no role in this result, based on the way modes share k-space. The useful dimensionless parameter is found to be $v = m_c / n^2$. An important result for applications is that the practical top mirror reflectivity R_1 that yields most of the extraction expected in the naive limit is given by $R_1^{\mathrm{crit}} = 1 - m_c/n^2$, generally well below 90%. This is sufficient to concentrate the extracted lobe (i.e., the outermost FP ring) into the escape cone. We also discussed how losses on the round-trip cavity path could possibly diminish the optimal top mirror reflectivity.

Spectral effects are important. We showed in Fig. 8 how brightness improvements first follow extraction improvements but then evolve differently depending of the source natural linewidth. Directionality is a consequence of strongly resonating cavities where, as a rule, front reflectivity R_1 is much closer to unity than R_1^{crit} and the source should be of sufficient purity. The tradeoffs between directionality, brightness enhancement B, and cavity order clearly appear in (17), $Bm_c\Delta\Omega = 4\pi$ where $\Delta\Omega$ is the the largest internal solid angle between that of the cavity mode and that deduced from the material emission linewidth.

Systems with DBR mirrors were studied introducing the penetration length which unfortunately increases cavity order according to $m_c = m_o + \Delta m_c$ [(23)]. An approximate critical number of DBR periods for the front mirror p^{opt} was given

in (26) and (28) for, respectively, symmetric and asymmetric cavities. Leaky modes have been analyzed in Appendix C. Adaptations to the small aperture case, e.g., for coupling to fibers, was also given in (30b).

In Part II [46], we introduce an exact approach to predict more accurately extraction of systems that could be used for real microcavity LED's, mainly focusing on an asymmetric DBR/cavity/metal structure. Selected parameters are varied in order to give a consistent set of performances for most existing semiconductors systems.

APPENDIX A
EFFECT OF LOSSES

As explained in Section II, losses can be assumed to be due to the back mirror and $1 - R_2$ taken as a parameter reflecting any loss per round-trip, whether they actually arise in the cavity itself or at the mirror. To go beyond the basic requirement $R_1 \leq R_2$, we have to sum the approximate Airy factor (T9) over angles. Neglecting again spectral width as well as the antinode factor, and with approximations in agreement with (11)–(13), one obtains for extracted power per emitter the following integral:

$$I \approx \int_0^{\theta_c} \frac{T_1}{(1 - r_1 r_2)^2 \left(1 + \frac{r_1 r_2}{(1 - r_1 r_2)^2}\left[\pi m_c(\theta^2 - \theta_o^2)\right]^2\right)} \theta \, d\theta$$

$$I \approx \frac{T_1}{(1 - r_1 r_2)} \frac{1}{\pi m_c \sqrt{r_1 r_2}} \arctan\left(\frac{\sqrt{r_1 r_2}}{(1 - r_1 r_2)} \pi m_c \theta_o^2\right) \tag{A1}$$

where the choice of the centered angle inside the escape cone, $\theta_o^2 \approx 1/2n^2$ (10), has been made. Analytical maximization of integral I (and hence of the extraction η within a factor) is unfortunately impossible due to the arctan function. But we can, without loss of generality, limit the number of parameters to two by calculating extraction enhancement over the bare case, $\eta/\eta_{\text{bare}} = \eta/(1/4n^2)$ or here $4In^2$ which then only depends on R_1, R_2, and the parameter $v = m_c/n^2$, according to

$$\frac{\eta}{\eta_{\text{bare}}} \approx \frac{4}{\pi} \frac{4(1 - R_1)}{(1 - \sqrt{R_1 R_2})(R_1 R_2)^{1/4}} \frac{1}{v}$$
$$\cdot \arctan\left(\frac{(R_1 R_2)^{1/4}}{(1 - \sqrt{R_1 R_2})} \frac{\pi}{2} v\right) \tag{A2}$$

where r_1, r_2, and T_1 have been expressed as a function of R_1 and R_2.

Results obtained upon maximizing (A2) for $v < 0.8$ and losses $(1 - R_2) < 0.3$ may be displayed as two contour maps in the $(1 - R_2, v)$ plane: contours of optimized R_1 [Fig. 12(a)] and contours of extraction enhancement η/η_{bare}, (A2) [Fig. 12(b)]. The resulting behavior for optimized R_1 respects the $R_1 < R_2$ prediction but may be considerably lower especially for large values of v, as explained in Section II-D. On the second map [Fig. 12(b)], enhancement contours are quite straight and parallel with a single constant slope (about -1.6, see below) in the useful range $v \geq 0.05$, allowing extraction to be described versus a single parameter if the
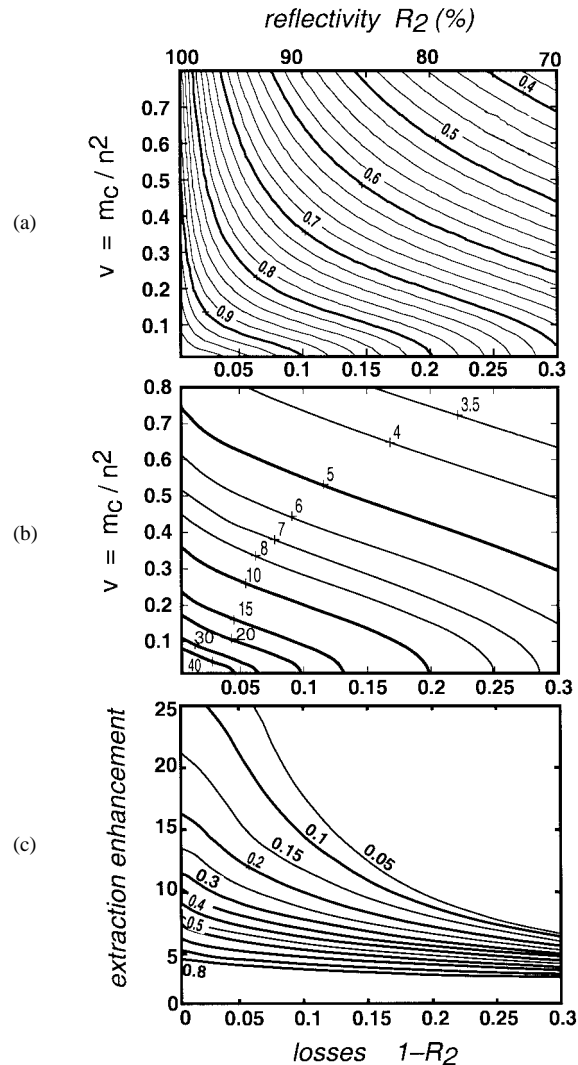

Fig. 12. (a) Optimized top mirror reflectivities R_1 contours in the $(1 - R_2, v = m_c/n^2)$ plane. (b) Optimized extraction enhancement $(\eta/\eta_{\text{bare}})$ contours in the same plane. (c) Extraction enhancement as a function of losses, for various values of parameter $v = m_c/n^2$. This is obtained from the results of (b) but can be transformed to the exact extraction of any particular case just by vertical rescaling.

optimization condition is fulfilled. When extraction gain from the shortened cavity is balanced by increased losses, as occurs when going from DBR to metallic back mirrors (see Section II-F), this simple law eases decision.

Extraction enhancement η/η_{bare} appears as the ordinate on Fig. 12(c) displaying in the $(1 - R_2, \eta/\eta_{\text{bare}})$ plane the very results of Fig. 12(b), but here as v-indexed contours. This map is closer to applications: one directly reads the obtained extraction enhancement stemming from the value of cavity parameter $v = m_c/n^2$, known from material and technological considerations, and the value of losses, known from mirror performances and possible intracavity losses. Absolute extraction is just obtained by multiplying the ordinate of Fig. 12(c) by the bare extraction, $\eta_{\text{bare}} = 1/4n^2$.

Analytical formulas demand additional approximations. When $(1 - R_2)v < 0.1$, we may take $(R_1 R_2)^{1/4} \approx 1$ in (A2), thus slightly underestimating extraction. Also, in the region of Fig. 12(b) with about constant slope, $\arctan(x) \approx \pi/2 - 1/x$

is acceptable in (A2). These approximations give

$$\frac{\eta}{\eta_{\text{bare}}} \approx \frac{8}{\pi v} \left(\frac{1 - R_1}{2 - R_1 - R_2} \right) \arctan \left(\frac{\pi v}{2 - R_1 - R_2} \right)$$

$$\approx \frac{4}{v} \left(\frac{1 - R_1}{2 - R_1 - R_2} \right) - \frac{8(1 - R_1)}{\pi^2 v^2}. \quad \text{(A3)}$$

This is readily maximized, yielding the following approximate optimized reflectivity R_1^{loss} and extraction enhancement

$$R_1^{\text{loss}} = 1 - T_1^{\text{loss}}$$

$$= (1 - R_2) + \left(1 - \pi \sqrt{(1 - R_2) \frac{v}{2}} \right) \quad \text{(A4)}$$

$$\left(\frac{\eta_{\text{max}}}{\eta_{\text{bare}}} \right) = \left(\frac{2}{\pi v} \left[\pi \sqrt{v} - \sqrt{2(1 - R_2)} \right] \right)^2. \quad \text{(A5)}$$

Still in this approximation, studying in the $(1 - R_2, v)$ plane constant $(\eta/\eta_{\text{bare}})$ enhancement curves analogous to those of Fig. 12(b), one finds an inflexion point located at

$$v_{\text{infl}} = \frac{9}{4} \left(\frac{\eta}{\eta_{\text{bare}}} \right)^{-1} \quad \text{(A6)}$$

$$1 - R_2 = \frac{3\pi^2}{16} \left(\frac{\eta}{\eta_{\text{bare}}} \right)^{1/2} \quad \text{(A7)}$$

characterized by a constant slope close to -1.6

$$\left(\frac{dv}{d(1 - R_2)} \right)_{v_{\text{infl}}} = -\frac{16}{\pi^2} \cong -1.6 \quad \text{(A8)}$$

which we use in the discussion of Section II-F to decide how much metal losses will still be acceptable due to the decreased cavity order in asymmetric metal/semiconductor/DBR microcavities.

APPENDIX B
SPECTRAL WIDTH AND SPONTANEOUS
EMISSION IN A MICROCAVITY

A. Angular Widths

Let us recall that θ_o denotes the angle of the extracted mode ($\theta_o < \theta_c$) for monochromatic radiation at k_o [refer to (T11)–(T13) of Table I to deal with the special case $\theta_o = 0$]. The internal angular width of this mode is denoted here $\Delta\theta_{\text{mono}}$ to avoid confusion and is obtained from the Airy denominator (T9e) by making $s = 0$ (since $k = k_o$) and requiring that $F^2 m_c^2 (\theta^2 - \theta_o^2) = 1$ for $\theta = \theta_o \pm \Delta\theta_{\text{mono}}/2$. One then finds (T11) and (T12a). Since θ_o is a small angle, the corresponding solid angle is $\Delta\Omega = \Delta\Omega_{\text{mono}} \approx \theta_o \times (2\pi\Delta\theta_{\text{mono}})$, hence (T12b).

As for the linewidth-limited angular width $\Delta\theta_{\text{poly}}$, it is obtained from the resonant angle evolution in approximate form, when requiring $\cos\theta/\cos\theta_o$ to reach $k/k_o = 1 \pm S/2$

$$(\theta^2 - \theta_o^2)/2 = \pm S/2 \quad \text{(B1)}$$

which yields

$$\Delta\theta_{\text{poly}} = S/\theta_o. \quad \text{(B2)}$$

Similarly, we have

$$\Delta\Omega_{\text{poly}} = \theta_o \times (2\pi\Delta\theta_{\text{poly}}) = 2\pi S. \quad \text{(B3)}$$

Four remarks can be made at this stage.

1) An optimized value for θ_o was argued to be $\theta_o = 1/\sqrt{2n}$. It can be reported into the above equations to yield internal angular widths.
2) For this case, the resonant angle being 45° in air, the useful outside angular widths, denoted $\Delta\theta'$, may be expressed from a differentiation of Snell's law as

$$\Delta\theta'_{\text{mono}} \approx 2n^2/Fm_c \quad \text{(B4)}$$

$$\Delta\theta'_{\text{poly}} \approx 2n^2 S \quad \text{(B5)}$$

[see (T14) for outside solid angle].
3) For resonance at normal incidence, one half of the FP peak is cut off (see Fig. 3), $\Delta\Omega$'s are halved, and angular widths are given by different formulas, e.g., (T13a), since in this case $\Delta\Omega \approx \pi\Delta\theta^2$.
4) For the practical working point of Section II-C, $R_1 = R_1^{\text{crit}}$, $\Delta\Omega'_{\text{mono}}$ is just $\sqrt{2}$ sterad and $\Delta\theta'_{\text{mono}} \approx 18° \approx 1/\pi$ rad, a value independent of index and cavity order.

B. Brightness and the Crossover

With these formulas, the crossover between the case $\Delta\theta_{\text{poly}} \ll \Delta\theta_{\text{mono}}$—where lobe brightness can still increase—and the converse case—where it saturates—is given by the three equivalent forms

$$SFm_c = 1 \quad \text{(B6)}$$

$$2\pi Sm_c = T_1 = 1 - R_1 \quad \text{(B7)}$$

$$2\pi S = \Delta\Omega_{\text{mono}}. \quad \text{(B8)}$$

The latter form clearly appears in Fig. 8 as the main diagonal.

The microcavity gives a brightness enhancement B of its resonant lobe (i.e., FP ring) over the no-cavity Lambertian emission. We first determine the enhancement B_{mono} in the monochromatic case. In the no-cavity case, the normalized internal power per steradian is just $1/4\pi$ (isotropic source) whereas in a lossless microcavity of sufficient front reflectivity ($R_1 \geq R_1^{\text{crit}}$), the fraction $1/m_c$ of emitted power is concentrated within the solid angle $\Delta\Omega_{\text{mono}} = F/2\pi m_c$, giving $F/2\pi$ for the normalized power per steradian. Hence, from the ratio, we have the two equivalent forms for the brightness enhancement

$$B_{\text{mono}} = 2F; \quad B_{\text{mono}}\Delta\Omega_{\text{mono}}m_c = 4\pi \quad \text{(B9)}$$

which is also (17).

Above the crossover, one follows the same approach, but the fraction $1/m_c$ of the emitted power is now concentrated over $\Delta\Omega_{\text{poly}} = 2\pi S$, hence the brightness enhancement now takes the following forms:

$$B_{\text{poly}} = 2/Sm_c; \quad B_{\text{poly}}\Delta\Omega_{\text{poly}}m_c = 4\pi \quad \text{(B10)}$$

yielding again (17) [32]–[34].

In between, around the crossover, one may use an integration of the Lorentzian form of the Airy function, which

is legitimated by the microcavity regime (small order m_c). Brightness enhancement B reads in this approach

$$B = \frac{4}{\pi S m_c} \arctan\left(\frac{2\pi S m_c}{1 - R_1}\right) = \frac{4}{S\pi m_c} \arctan(FSm_c)$$

(B11)

which reduces to the above equations for $FSm_c \ll 1$ (monochromatic case) or $FSm_c \gg 1$ (polychromatic case). Let us finally emphasize that the calculated enhancement also holds for outside radiation even though it was calculated from the internal point of view.

C. Very Large Spectral Width and Extraction

A large spectral width S translates into an angular spread exceeding the $[0 \rightarrow \theta_c]$ escape window. Noting that $\cos(\theta_c) \approx 1 - 1/2n^2$, it is obvious that if S exceeds the value

$$S_{\mathrm{esc}} = 1/2n^2$$

(B12)

which is typically 3%–10%, a cavity enhances only a part of the source spectrum outside and inhibits other frequencies (see Section II-G for smaller aperture requirements where a similar effect arises). For S largely exceeding S_{esc} (very strong pumping, long wavelength, ...), benefits from microcavity for extraction clearly decrease. But by using epoxy as the outer medium, one has the possibility to increase the threshold linewidth S_{esc} by a factor of more than two ($n^2 \approx 2.25$), gaining, thus, a comfortable margin where microcavities are still interesting. With this provision, i.e., when we have $S < 1/2n^2$, the spread in internal angles is smaller than θ_c so that all wavelengths are extracted at some angle. But this is no more true in the large spectral width limit which we consider here for completeness [Fig. 7(c)]. Using Fig. 3, we replace the ring $k = k_o$ by a thick annulus. It is here so thick that some wavelengths never lie into the resonant outgoing FP peak. Obviously, only a fraction S_{esc}/S may lie in this peak. It is then clear that extraction follows at first order the ratio S_{esc}/S of extracted to total spectral width, being thus of order

$$\eta = S_{\mathrm{esc}}/(Sm_c) = 1/(2Sn^2 m_c).$$

(B13)

It is interesting in this case to parallel for spectral width the approach made when defining R_1^{crit} through angular variations of the Airy denominator. We now want this denominator to increase by $\sim\pi^2$ for the extreme radiations $k = k_o \pm \Delta k/2$, i.e., $s = \pm S/2$, instead of an angular variation. One gets a spectral-width-wise critical transmission $T_1^{\mathrm{sp, crit}} = 2Sm_c$ and the associated critical reflectivity is

$$R_1^{\mathrm{sp, crit}} = 1 - 2Sm_c.$$

(B14)

This latter value falls below R_1^{crit} if $S > S_{\mathrm{esc}} = 1/2n^2$, in agreement with the discussion. As for the brightness, the first form of (B10) still holds. In the somewhat extreme limit $S = 1$, it yields a factor of two due to the mere back-mirror power reflection. However, due to the numerous approximations made, such formulas should be taken as guidelines when $S \gg S_{\mathrm{esc}}$.
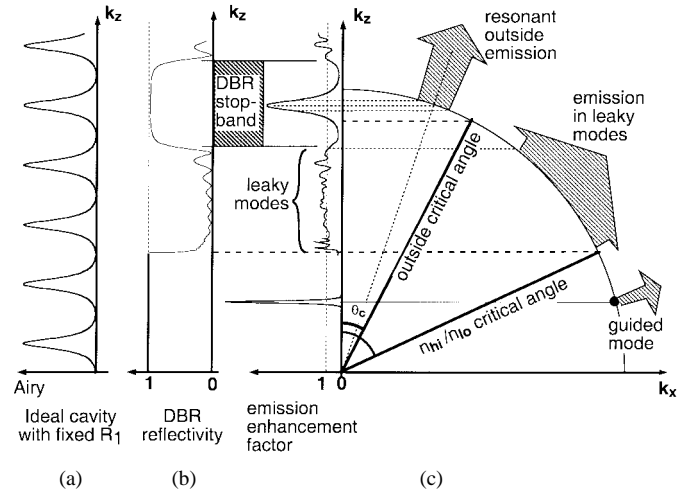

Fig. 13. Same plot as Figs. 3 and 4 when using DBR mirrors. (a) Comb-like Airy function of an ideal cavity with constant reflectivities. (b) DBR reflectivity, with the stopband, the window at smaller k_z and the about total reflection at critical angle with the low index medium. (c) Modified Airy function, with the extracted FP peak, but losing the structure of (a) especially in the leaky mode region. Emission in the various modes is indicated.

APPENDIX C
STOPBAND AND LEAKY MODES OF DBR STRUCTURES

When a DBR with moderate-index step is used on a high-index substrate as the output side (the wafer being eventually antireflection coated, but far from the cavity), its limited angular acceptance allows light to escape toward the substrate at oblique angles still larger than θ_c, referred to as "leaky modes" [17], [18], [39], [40], [44], [64], [65]. We discuss here the main trends that can be predicted for these modes and how we can picture them in the k_x–k_z diagram of Fig. 3.

Let us first broadly define three regions in this diagram (Fig. 13): We start from the same k_x–k_z diagram as Fig. 3 [Fig. 13(c)] with the critical angle for outside radiation. The regular comb of the Airy function due to cavity round trips with angle-independent reflectivities is illustrated in Fig. 13(a). Whether the cavity is made from two similar DBR's or a metal and a DBR mirror, the power reflectivity product that enters into the Airy function has the typical shape of a DBR reflectivity of Fig. 13(b), with a stopband surrounded by an oscillating small reflectivity region around it. At larger angles (smaller k_z), there is again a unit reflectivity region due to the fact that we view the DBR from the high-index medium of the cavity. Thus, as indicated in Fig. 13(c) where angles are counted in the cavity medium, there is a critical angle θ_{lo} beyond which only evanescent waves are present in the DBR low-index medium, and the reflection becomes 100% toward the cavity. Let us discuss these three regions (stopband, leaky modes, and total reflection from the DBR) as well as the interplay between them and their possible design rules.

In the stopband region, the cavity just mimics a perfect one, with the same enhancement and inhibition of the Airy function. One should thus again, to extract as much light as possible, aim at fitting a single mode in the center of the k_z escape window corresponding to outside-coupled angles. For this purpose, the DBR stopband has to cover this window as well as possible. The DBR stopband center is determined

by the sole DBR layer thicknesses. On the other hand, the resonant mode position depends essentially on the bare cavity thickness [57], [60], [19]. Finally, the width of the resonant mode depends on the cavity finesse, which is given in the stopband by the number of DBR pairs (until other losses limit the finesse) via mirror reflectivities. The situation pictured in Fig. 13 is close to the preferred "working point" (R_1^{crit}), with a moderately high FP peak, but still fairly concentrating the power into the escape window.

Here only one FP mode is found through the stopband. But for larger stopbands or larger bare cavities, the stopband may contain more than one mode. The relevant mode spacing here is that of the compound cavity, including the penetration lengths of DBR's, (or equivalently, taking their linear phase response of Fig. 9(b) into account to obtain the round-trip phase condition). It is also important that the stopband is centered on the extracted mode. Otherwise, if the mode lies close to a stopband edge, a longer penetration length into the DBR results, hence a larger effective cavity order and a diminished extraction. For stopbands much larger than the escape window (large index contrasts), one part of the stopband thus lies at $k_z > k_o$, where it would be naive and useless to forbid emission.

What happens in the converse case of small index contrast where the stopband width is narrower than the escape window? Noticing that this corresponds approximately in relative terms to $(2\Delta n/\pi n) < 1/2n^2$, this means thus $n\Delta n < \pi/4$, which approximately amounts to violate the microcavity criterion for DBR-bounded cavities ($n\Delta n > 1/2$). We then enter the meso-cavity regime. The extraction coefficient is thus no more the microcavity regime one ($\eta = 1/m_c = \Delta n/2n$) because two or more resonant modes may take place into the escape window. Referring to the mode-countings arguments developed in Figs. 3–4, there is in this case not much room for the extraction enhancement, which will necessarily be less than a factor of two. A more quantitative prediction can be devised in this meso-cavity case using the ratio of the number of modes in the escape window to the total number of modes ($\sim\Delta n/n$), and leads to an asymptotic extraction enhancement of the form $(1 + An\Delta n)$ over the trivial power reflection effect ("far mirror"), the coefficient A being of order unity.

In the adjacent regions, those of leaky modes, cavity modes do not appear at all because the reflectivity product is small in the Airy function. Only complex oscillations due to the interplay of the peculiar phase response of the DBR with the bare cavity round-trip phase are visible. In the optimized case of Fig. 13, the solid angle subtended by leaky modes is just given by $\Omega_{\text{gui}} = 4\pi(\cos\theta_1 - \cos\theta_{\text{lo}})$ where the first angle denotes here the bottom of the DBR stopband. Since we have the identities $\cos\theta_1 \approx 1 - (1/4n^2) - (\Delta n/\pi n)$ and $\sin\theta_{\text{lo}} = n_{\text{lo}}/n = (n - \Delta n)/n$, we can thus conclude that the fraction of the solid angle for leaky modes is

$$\frac{\Omega_{\text{leaky}}}{4\pi} \approx 1 - \frac{1}{4n^2} - \frac{\Delta n}{\pi n} - \sqrt{1 - \left(\frac{n - \Delta n}{n}\right)^2}. \quad \text{(C1)}$$

It is plotted in Fig. 14 as a function of Δn for $n = 2, 3,$ and 4. For example, it is 33% only in the case $n = 3.5$, $\Delta n =$
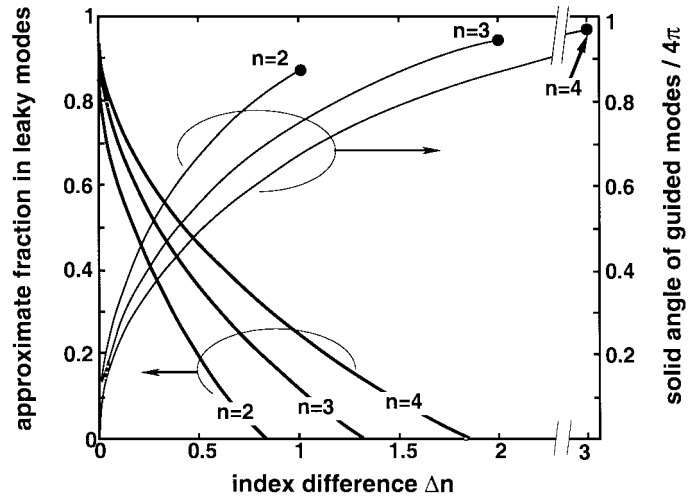

Fig. 14. Left scale: approximate fraction of emission in leaky modes calculated from the subtended solid angle as a function of Δn for high index $n = n_{\text{hi}} = 2, 3,$ and 4. On the right is the normalized solid angle where guided modes occur for comparison. The total is below unity because extracted modes are not included.

0.6, where the last term, in excess of one half, is crucial in determining the result. This simplified picture is modified in the two following cases.

1) Close to the DBR critical angle θ_{lo}, Fresnel reflection coefficients become large even though Δn may be weak. Thus the shorter bare cavity may at this stage act as a peaked FP cavity. An overall account of the transmission and reflection windows in this complex region is beyond our scope. It is analogous to the problem of Bloch waves in a square potential with minibands, etc. [59], [66], [67].

2) Substrate lift-off [5], [6]: in most light emitting devices, leaky modes are lost because the emitted light eventually reaches the substrate where it is often absorbed. One remedy is to remove the substrate to deposit the sole heterostructure layers on a low index substrate, causing total internal reflection at the angles of these leaky modes (the further interaction of these modes with the possibly absorptive emittor may cause some reabsorption and photon recycling, see [46]). In the new lift-off structure, almost all the modes of large angles are indeed guided modes of the detached layer stack. Then, the emission pattern of the previously leaky modes turns into a discrete one, but the cavity size is larger than at normal incidence since waves make round trips with unattenuated amplitude throughout both mirrors (we have, say, a configuration $R_2 =$ thicker DBR/bare cavity and $R_1 =$ thinner DBR) instead of being limited by the DBR penetration length at normal incidence. Teeth of the corresponding mode "comb" thus lie closer. However, on the average, overall emission in these modes has no reason to largely differ from the "ordinary" leaky mode emission, e.g., that calculated in [46].

Let us finally discuss spectral aspects: how do leaky modes vary for other wavelengths than the resonant one of Fig. 13? If, slightly abusively, we term "leaky modes" all the emission between both critical angles whatever its origin, then detuning

to the short wavelength side of the resonance gives rise to an important enhancement of these leaky modes: for this detuning, the resonant mode finally goes beyond the critical angle, causing a much stronger contribution than that of an isotropic source. On the contrary, detuning to the long wavelength side does not usually cause such an increase. See [46, Fig. 5] for details.

The last class of modes are akin to truly guided modes, with an angle larger than DBR critical angle θ_{lo}. In this class, round trips essentially take place in the bare cavity. Even if the substrate has the same index as the cavity, tunneling through low index layers is the only mechanism allowing coupling to radiative substrate modes. Given the thickness of low index layers, the exponential decay at the angles of concern is so important that these modes can hardly be distinguished from true guided modes with zero coupling to the outside world. On this basis, the "comb" made by these modes is usually very largely spaced since the bare cavity is generally narrow (m_o seldom exceeds 3 or 4, i.e., at most a 2λ cavity) [16], [18]. Notice, however, that even for the shortest high-index cavity ($\lambda/2$), the structure always sustains a guided mode, and that this guided mode tends to carry away a very large fraction of spontaneous emission, as is suggested by the large solid angle Ω_{gui} between θ_{lo} and the equator $\theta = \pi/2$. However, for short bare cavities bounded with DBR mirrors, the guided power fraction may largely deviate from the ratio $\Omega_{\text{gui}}/4\pi$, especially at large index contrasts Δn: such cavities have very few modes among which a strong resonating mode close to normal incidence and the fraction in the guided mode is the result of a somewhat complex competition between these modes. As a rule, the fraction of power in guided modes at large Δn, when leaky modes tend to a small fraction, is complementary to the power in outside modes, being diminished for structures with enhanced extraction and enhanced in the converse case of a structure inhibiting emission in the escape window, e.g., a $3\lambda/4$ cavity between two DBR's. These approximate trends are quantified in a particular case in [46, Fig. 5].

ACKNOWLEDGMENT

REFERENCES

[1] G. B. Stringfellow and M. G. Craford, Eds., *High-Brightness Light-Emitting Diodes*. San Diego, CA: Academic, 1997, p. 48.

[2] M. G. Craford, "Commercial light emitting diode technology: Status, trends and possible future performances," in *Microcavities and Photonic Bandgaps: Physics and Application*, J. Rarity and C. Weisbuch, Eds. Dordrecht, The Netherlands: Kluwer, 1996, pp. 323–332.

[3] W. N. Carr, "Photometric figures of merit for semiconductor luminescent sources operating in spontaneous mode," in *Semiconductor Devices Pioneering Papers*, S. M. Sze, Ed. London, U.K.: World Scientific, 1991, pp. 919–937.

[4] F. A. Kish, F. M. Steranka, D. C. DeFevere, D. A. Vanderwater, K. G. Park, C. P. Kuo, T. D. Osentowski, M. J. Peanasky, J. G. Yu, R. M. Fletcher, D. A. Steigerwald, M. G. Craford, and V. M. Robbins, "Very-high efficiency semiconductor wafer-bonded transparent-substrate $(Al_xGa_{1-x})_{0.5}In_{0.5}$P/GaP light-emitting diodes," *Appl. Phys. Lett.*, vol. 64, pp. 2839–2841, 1994.

[5] G. E. Höfler, D. A. Vanderwater, D. C. DeFevere, F. A. Kish, M. D. Camras, F. M. Steranka, and I. H. Tan, "Wafer bonding of 50-mm diameter GaP to AlGaInP-GaP light-emitting diode wafers," *Appl. Phys. Lett.*, vol. 69, pp. 803–805, 1996.

[6] C. Brys, F. Vermaerke, P. Demeester, P. V. Daele, K. Rakennus, A. Salokatve, P. Uusimaa, M. Pessa, A. L. Bradley, J. P. Doran, J. O'Gorman, and H. Hegarty, "Epitaxial lift-off of ZnSe based II-VI structures," *Appl. Phys. Lett.*, vol. 66, pp. 1086–1088, 1995.

[7] G. Gu, D. Z. Garbuzov, P. E. Burrows, S. Venkatesh, and S. R. Forrest, "High-external-quantum efficiency organic light-emitting devices," *Opt. Lett.*, vol. 22, pp. 396–398, 1997.

[8] I. Schnitzer, E. Yablonovitch, C. Caneau, and T. J. Gmitter, "Ultrahigh spontaneous emission quantum efficiency, 99.7% internally and 72% externally, from AlGaAs/GaAs/AlGaAs double heterostructures," *Appl. Phys. Lett.*, vol. 62, pp. 131–133, 1993.

[9] H. De Neve, J. Blondelle, P. Vandaele, P. Demeester, R. Baets, and G. Borghs, "Recycling of guided mode light emission in planar microcavity light emitting diodes," *Appl. Phys. Lett.*, vol. 70, pp. 799–801, 1997.

[10] J. L. Bradshaw, R. P. Devaty, W. J. Choyke, and R. L. Messham, "Below-band-gap photon recycling in $Al_xGa_{1-x}As$," *Appl. Phys. Lett.*, vol. 55, pp. 165–167, 1989.

[11] T. Nishikawa, T. Kakimura, Y. Lee, and M. Yamanishi, "Enhanced transfer efficiency in AlGaAs asymmetric planar microcavities," *Appl. Phys. Lett.*, vol. 65, pp. 1796–1798, 1994.

[12] T. Nishikawa, M. Yokota, S. Nakamura, Y. Kadoya, M. Yamanishi, and I. Ogura, "Influence of photon reabsorption on the transfer efficiency of output intensity in semiconductor microcavities," *IEEE Photon. Technol. Lett.*, vol. 9, pp. 179–181, 1997.

[13] I. Schnitzer, E. Yablonovitch, C. Caneau, T. J. Gmitter, and A. Scherer, "30-percent external quantum efficiency from surface textured, thin-film light-emitting-diodes," *Appl. Phys. Lett.*, vol. 63, pp. 2174–2176, 1993.

[14] R. E. Slusher and C. Weisbuch, "Optical microcavities in condensed matter systems," *Solid. State Commun.*, vol. 92, pp. 149–155, 1994.

[15] N. E. J. Hunt, E. F. Schubert, R. A. Logan, and G. J. Zydzik, "Enhanced spectral power density and reduced linewidth at 1.3 μm in an InGaAsP quantum well resonant cavity light-emitting diode," *Appl. Phys. Lett.*, vol. 61, pp. 2287–2289, 1992.

[16] N. E. J. Hunt, E. F. Schubert, D. L. Sivco, A. Y. Cho, R. F. Kopf, R. A. Logan, and G. J. Zydzik, "High efficiency, narrow spectrum resonant-cavity light-emitting diodes," in *Confined Electrons and Photons*, E. Burstein and C. Weisbuch, Eds. New York: Plenum, 1995, pp. 703–714.

[17] D. G. Deppe and C. Lei, "Spontaneous emission from a dipole in a semiconductor microcavity," *J. Appl. Phys.*, vol. 70, pp. 3443–3448, 1991.

[18] H. De Neve, J. Blondelle, R. Baets, P. Demeester, P. Vandaele, and G. Borghs, "High efficiency planar microcavity LEDs: Comparison of design and experiments," *IEEE Photon. Technol. Lett.*, vol. 7, pp. 287–289, 1995.

[19] J. Blondelle, H. De Neve, P. Demeester, P. Vandaele, G. Borghs, and R. Baets, "16% external quantum efficiency from planar microcavity LED's at 940 nm by precise matching of cavity wavelength," *Electron. Lett.*, vol. 31, pp. 1286–1287, 1995.

[20] ———, "6-percent external quantum efficiency from InGaAs/(Al)GaAs single-quantum-well planar microcavity LED's," *Electron. Lett.*, vol. 30, pp. 1787–1788, 1994.

[21] E. F. Schubert, N. E. J. Hunt, R. J. Malik, M. Micovic, and D. L. Miller, "Temperature and modulation characteristics of resonant-cavity light-emitting diodes," *J. Lightwave Technol.*, vol. 14, pp. 1721–1728, 1996.

[22] H. De Neve, J. Blondelle, P. Vandaele, P. Demeester, R. Baets, and G. Borghs, "Planar substrate-emitting microcavity light emitting diodes with 20% external QE," presented at SPIE Photonics West, San Jose, CA, 1997.

[23] J. Blondelle, H. De Neve, G. Borghs, P. Vandaele, P. Demeester, and R. Baets, "High efficiency (>20%) microcavity LED's," in *Proc. IEE Coll. on Semiconductor Optical Microcavity Devices and Photonic Bandgaps*, London, U.K., 1996.

[24] H. De Neve, "Study and realization of microcavity based LED's," Ph.D. dissertation, Univ. of Gent, Belgium, 1997.

[25] J. Blondelle, "Realization of high-efficiency substrate-emitting In-GaAs/(Al)GaAs microcavity LED's by means of MOCVD," Ph.D. dissertation, Univ. of Gent, Belgium, 1997.

[26] E. Hadji, J. Bleuse, N. Magnea, and J.-L. Pautrat, "3.2 μm infrared resonant cavity light-emitting diode," *Appl. Phys. Lett.*, vol. 67, pp. 2591–2593, 1995.

[27] E. F. Schubert, Y. H. Wang, A. Y. Cho, L. W. Tu, and G. J. Zydzik, "Resonant cavity light-emitting diode," *Appl. Phys. Lett.*, vol. 60, pp. 921–923, 1992.

[28] K. Neyts, "Cavity effects in thin film phosphors based on ZnS," in *Microcavities and Photonic Bandgaps: Physics and Applications*, J. Rarity and C. Weisbuch, Eds. Dordrecht, The Netherlands: Kluwer, 1996, pp. 397–406.

[29] U. Lemmer *et al.*, "Microcavity effects in a spin-coated polymer 2-layer system," *Appl. Phys. Lett.*, vol. 66, pp. 1301–1303, 1995.

[30] N. Takada, T. Tsutsui, and S. Saito, "Strongly directed emission from controlled-spontaneous-emission electroluminescent diodes with europium complex as an emitter," *Jpn. J. Appl. Phys.*, vol. 33, pp. L863–L866, 1994.

[31] ——, "Strongly-directed emission from microcavity structure in electroluminescent diodes with europium complex as an emitter," *Synthetic Metals*, vol. 71, pp. 2099–2100, 1995.

[32] N. E. J. Hunt, A. M. Vredenberg, E. F. Schubert, E. F. Becker, D. C. Jacobson, J. M. Poate, and G. J. Zydzik, "Spontaneous emission control in planar structures: Er^{3+} in Si/SiO$_2$ microcavities," in *Confined Electrons and Photons*, E. Burstein and C. Weisbuch, Eds. New York: Plenum, 1995, pp. 703–714.

[33] K. Ujihara, "A simple relationship between directivity and linewidth of a planar microcavity laser," *Jpn. J. Appl. Phys.*, vol. 33, pp. 1059–1060, 1994.

[34] ——, "Spontaneous emission in a micro optical cavity from spectrally broadened atoms," *Opt. Commun.*, vol. 103, pp. 265–276, 1993.

[35] T. Tsutsui, N. Takada, and S. Saito, "Control of spontaneous emission using microcavity structures in organic electroluminescent devices," *Synthetic Metals*, vol. 71, pp. 2001–2004, 1995.

[36] D. L. Huffaker, C. Lei, D. G. Deppe, C. J. Pinzone, J. G. Neff, and R. D. Dupuis, "Controlled spontaneous emission in room temperature semiconductor microcavities," *Appl. Phys. Lett.*, vol. 60, pp. 3203–3205, 1992.

[37] Z. Huang, C. C. Lin, and D. G. Deppe, "Spontaneous lifetime and quantum efficiency in light-emitting-diodes affected by a close metal mirror," *IEEE J. Quantum Electron.*, vol. 29, pp. 2940–2949, 1993.

[38] S. D. Brorson, H. Yokoyama, and E. Ippen, "Spontaneous emission rate alteration in optical waveguide structures," *IEEE J. Quantum Electron.*, vol. 26, pp. 1492–1499, 1990.

[39] G. Björk, S. Machida, Y. Yamamoto, and K. Igeta, "Modification of spontaneous emission rate in planar dielectric microcavity structures," *Phys. Rev. A*, vol. 44, pp. 669–681, 1991.

[40] H. Yokoyama and K. Ujihara, Eds., *Spontaneous Emission and Laser Oscillation in Microcavities*. Boca Raton, FL: CRC Press, 1995.

[41] C. Weisbuch, M. Nishioka, A. Ishikawa, and Y. Arakawa, "Observation of the coupled exciton-photon mode splitting in a semiconductor quantum microcavity," *Phys. Rev. Lett.*, vol. 69, pp. 3314–3317, 1992.

[42] Y. Yamamoto, F. Matinaga, S. Machida, A. Karlsson, J. Jacobson, G. Björk, and T. Mukai, "Quantum-electrodynamic effects in semiconductor microcavities—Microlasers and coherent exciton-polariton emission," *J. Phys. IV*, vol. 3, pp. 39–46, 1993.

[43] R. P. Stanley, R. Houdré, C. Weisbuch, U. Oesterle, and M. Ilegems, "Cavity polariton photoluminescence in semiconductor microcavities: Experimental evidence," *Phys. Rev. B*, vol. 53, pp. 10995–11007, 1996.

[44] J. Rarity and C. Weisbuch, Eds., *Microcavities and Photonic Bandgaps: Physics and Applications*, NATO ASI Series E324. Dordrecht, The Netherlands: Kluwer, 1996.

[45] R. Houdré, R. P. Stanley, and M. Ilegems, "Strong coupling regime in the presence of inhomogeneous broadening: Resolution of an homogeneous linewidth in an inhomogeneously broadened system," *Phys. Rev. A*, vol. 53, pp. 2711–2715, 1996.

[46] H. Benisty, H. De Neve, and C. Weisbuch, "Impact of planar microcavity effects on light extraction—Part II: Selected exact simulations and role of photon recycling," this issue, pp. 1632–1643.

[47] A. Kastler, "Atomes à l'intérieur d'un interféromètre Perot-Fabry," *Appl. Opt.*, vol. 1, pp. 17–24, 1962.

[48] W. Lukosz, "Theory of optical-environment-dependent spontaneous-emission rates for emitters in thin layers," *Phys. Rev. B*, vol. 22, pp. 3030–3038, 1980.

[49] D. G. Deppe and C. Lei, "Spontaneous emission and optical gain in a Fabry-perot microcavity," *Appl. Phys. Lett.*, vol. 60, pp. 527–529, 1992.

[50] M. Born and E. Wolf, *Principles of Optics*. Oxford, U.K.: Pergamon, 1970.

[51] B. E. A. Saleh and M. C. Teich, *Fundamental of Photonics*, Wiley series in pure and applied optics. New York: Wiley, 1991.

[52] G. Björk, "On the spontaneous lifetime change in an ideal planar microcavity—Transition from a mode continuum to quantized modes," *IEEE J. Quantum Electron.*, vol. 30, pp. 2314–2318, 1994.

[53] K. Ujihara, "Spontaneous emission and the concept of effective area in a very short optical cavity with plane parallel dielectric mirrors," *Jpn. J. Appl. Phys.*, vol. 30, pp. L901–L904, 1991.

[54] R. Baets, P. Demeester, and P. E. Lagaase, "High-reflectivity GaAs-AlGaAs mirrors: Sensitivity analysis with respect to epitaxial growth parameters," *J. Appl. Phys.*, vol. 62, pp. 723–726, 1987.

[55] A. Salokatve, K. Rakennus, P. Uusimaa, M. Pessa, T. Aherne, J. P. Doran, J. O'Gorman, and J. Hegarty, "Growth and characterization of an epitaxially grown ZnSSe/MnZnSSe distributed Bragg reflector," *Appl. Phys. Lett.*, vol. 67, pp. 407–409, 1995.

[56] U. Oesterle, R. P. Stanley, R. Houdré, M. Gailhanou, and M. Ilegems, "Molecular beam epitaxy of an ultrahigh finesse microcavity," *J. Cryst. Growth*, vol. 150, pp. 1313–1317, 1995.

[57] R. P. Stanley, R. Houdré, U. Oesterle, and M. Ilegems, "Impurity modes in one-dimensional periodic-systems: The transition from photonic band-gaps to microcavities," *Phys. Rev. A*, vol. 48, pp. 2246–2250, 1993.

[58] D. L. Huffaker, C. C. Lin, D. G. Deppe, B. G. Streetman, and T. J. Rogers, "Mode dependence on mirror contrast in Fabry-Perot microcavity lasers," *IEEE Photon Technol. Lett.*, vol. 6, pp. 135–138, 1994.

[59] P. Yeh, *Optical Waves in Layered Media*. New York: Wiley, 1988.

[60] H. A. McLeod, *Thin-Film Optical Filters*. Bristol, U.K.: Adam Hilger, Ltd., 1986.

[61] A. Yariv, *Optical Electronics*, 4th ed. Orlando, FL: Saundeers, 1991.

[62] N. W. Ashcroft and N. D. Mermin, *Solid State Physics*. Fort Worth, TX: Harcourt Brace, 1976.

[63] C. Kittel, *Quantum Theory of Solids*. New York: Wiley, 1987.

[64] G. Björk, H. Heitmann, and Y. Yamamoto, "Spontaneous-emission coupling factor and mode characteristics of planar dielectric microcavity lasers," *Phys. Rev. A*, vol. 47, pp. 4451–4463, 1993.

[65] T. Baba, T. Hamano, F. Koyama, and K. Iga, "Spontaneous emission factor of a microcavity DBR surrface emitting laser," *IEEE J. Quantum Electron.*, vol. 27, pp. 1347–1358, 1991.

[66] A. Yariv and P. Yeh, *Optical Waves in Crystals*. New York: Wiley, 1984.

[67] E. Burstein and C. Weisbuch, Eds., *Confined Electrons and Photons*, NATO ASI Series B340. Boston, MA: Plenum, 1995.

H. Benisty, photograph and biography not available at the time of publication.

H. De Neve, photograph and biography not available at the time of publication.

C. Weisbuch, photograph and biography not available at the time of publication.